THE JOURNAL OF BIOLOGICAL CHEMISTRY VOL. 290, NO. 41, pp. 24858–24874, October 9, 2015
Published in the U.S.A.

CD47 Receptor Globally Regulates Metabolic Pathways That Control Resistance to Ionizing Radiation*[S]

Received for publication, May 18, 2015, and in revised form, August 26, 2015 Published, JBC Papers in Press, August 26, 2015, DOI 10.1074/jbc.M115.665752

Thomas W. Miller[‡§1], **David R. Soto-Pantoja**[‡¶1,2], **Anthony L. Schwartz**[‡], **John M. Sipes**[‡], **William G. DeGraff**[‖], **Lisa A. Ridnour**[‖], **David A. Wink**[‖], and **David D. Roberts**[‡3]

From the [‡]*Laboratory of Pathology and* [‖]*Radiation Biology Branch, Center for Cancer Research, NCI, National Institutes of Health, Bethesda, Maryland 20892,* [§]*Paradigm Shift Therapeutics, Rockville, Maryland 20852, and* [¶]*Departments of Cancer Biology and Hypertension and Vascular Research Center, Wake Forest School of Medicine, Winston-Salem, North Carolina 27157*

Background: CD47 is a widely expressed receptor that regulates cellular responses to stress.
Results: CD47 regulates metabolic pathways required to control glucose metabolism, oxidative stress, DNA repair, and energetics after exposure to ionizing radiation.
Conclusion: CD47 broadly limits the capacity of cells and tissues to survive and recover from damage caused by ionizing radiation.
Significance: CD47-targeted therapeutics could be global regulators of cell metabolism.

Modulating tissue responses to stress is an important therapeutic objective. Oxidative and genotoxic stresses caused by ionizing radiation are detrimental to healthy tissues but beneficial for treatment of cancer. CD47 is a signaling receptor for thrombospondin-1 and an attractive therapeutic target because blocking CD47 signaling protects normal tissues while sensitizing tumors to ionizing radiation. Here we utilized a metabolomic approach to define molecular mechanisms underlying this radioprotective activity. CD47-deficient cells and *cd47*-null mice exhibited global advantages in preserving metabolite levels after irradiation. Metabolic pathways required for controlling oxidative stress and mediating DNA repair were enhanced. Some cellular energetics pathways differed basally in CD47-deficient cells, and the global declines in the glycolytic and tricarboxylic acid cycle metabolites characteristic of normal cell and tissue responses to irradiation were prevented in the absence of CD47. Thus, CD47 mediates signaling from the extracellular matrix that coordinately regulates basal metabolism and cytoprotective responses to radiation injury.

Cell and tissue responses to stress are key determinants of the outcome of many disease processes. In multicellular organisms, programmed cell death can be an appropriate response to genotoxic stress to limit the accumulation of genomic mutations that could result in malignancies (1). However, therapeutics that minimize the off target cell death caused by cytotoxic chemotherapy and radiation therapy are also needed for treating cancer.

Resistance to stress can be conferred by activation of protective processes such as autophagy and DNA damage repair pathways (2). These processes are accompanied by a metabolic reprogramming that preserves scarce nutrients and initiates repair or degradation of damaged cell components (3). Several studies have systematically defined the metabolic changes that are induced in cells and live animals exposed to low or high doses of ionizing radiation (IR).[4] High dose radiation results in the loss of metabolites associated with oxidative stress and DNA damage responses (4). These metabolic alterations include accumulation of degradation products derived from oxidized membrane lipids and damaged DNA, loss of glutathione and NADH, and induction of precursors involved in nucleotide biosynthesis that are required for DNA repair (4–7). In animals, the metabolic changes associated with IR injury have largely been measured indirectly by assessing changes in serum or excreted urinary metabolites, which can be employed as biomarkers for radiation damage (8–11). Changes in tissue metabolite levels are often inversely related to those measured in serum (12).

In the context of therapeutic irradiation for treating cancer, an ideal outcome would be to maximize cell death responses in irradiated tumor tissue while protecting nearby healthy tissues. General radioprotectants such as the radical scavenger amifostine show some specificity for selectively protecting healthy

* This work was supported, in whole or in part, by National Institutes of Health Projects ZIASC009172, ZIA BC 010898, and ZIASC009174 (Intramural Research Program of the NCI; to D. D. R. and D. A. W), an NCI Director's Career Development Innovation Award (to T. W. M.), and by the NCI Office of Biotechnology Partnerships (to D. S.-P.). This work was also supported by the Avon Foundation (to T. W. M.). The authors declare that they have no conflicts of interest with the contents of this article.
[S] This article contains supplemental Table 1.
[1] Both authors were equal contributors.
[2] To whom correspondence may be addressed: Dept. of Cancer Biology and Hypertension and Vascular Research Center, Wake Forest School of Medicine, Winston-Salem, NC 27157. Tel.: 336-716-0792; Fax: 336-716-2456; E-mail: dsotopan@wakehealth.edu.
[3] To whom correspondence may be addressed: NIH, Bldg. 10 Rm. 2A33, 10 Center Dr. MSC1500, Bethesda, MD 20892-1500. Tel.: 301-594-5256; Fax: 301-402-0043; E-mail: droberts@helix.nih.gov.

[4] The abbreviations used are: IR, ionizing radiation; Gy, gray; GATM, glycine amidinotransferase; GLUT1, glucose transporter isoform-1; LIMS, laboratory information management system; MTS, [3-(4,5-dimethylthiazol-2-yl)-5-(3-carboxymethoxyphenyl)-2-(4-sulfophenyl)-2H-tetrazolium, inner salt; NAALAD2, *N*-acetylated α-linked acidic dipeptidase-2; NBDG, 2-(*N*-(7-nitrobenz-2-oxa-1,3-diazol-4-yl)amino)-2-deoxyglucose; OCR, oxygen consumption rate; PGC1α, peroxisome proliferator-activated receptor-γ coactivator-1α; PPP, pentose phosphate pathway; UPLC, ultrahigh performance liquid chromatography; ANOVA, analysis of variance; Gpx1, glutathione peroxidase-1.

cells (13) but have not extended cancer patient survival in the context of radiotherapy (14). Targeting repair pathways that are dysregulated in the context of mutated oncogenes and tumor suppressor genes is one promising approach to achieve selective radioprotection but requires much further development (6, 15–17).

We have identified a novel signaling pathway controlled by the extracellular environment that modulates cell responses to a variety of stresses. Mice lacking the secreted glycoprotein thrombospondin-1 or its cell surface signaling receptor CD47 are remarkably resistant to fixed ischemic injuries, ischemia/reperfusion injury, and exposure to high doses of IR (18, 19). Pharmacological blockade of CD47 in wild type (WT) mice protects radiosensitive tissues and increases survival of lethal total body irradiation (20, 21). Radioresistance is an intrinsic property of thrombospondin-1 or *cd47*-null cells, and temporary disruption of CD47 signaling induces radioresistance in WT cells (19, 20). The radioresistance of *cd47*-null cells or blockade of CD47 in WT cells requires induction of protective autophagy (22). Moreover, studies in tumor-bearing mice revealed that, although normal tissues and tumor associated $CD8^+$ T cells in these mice are protected from radiation injury, irradiated tumors show increased $CD8^+$ T cell-dependent therapeutic ablation after CD47 blockade (20, 23). Thus, the CD47 pathway is a promising therapeutic target to enhance the efficacy of tumor irradiation while minimizing damage of critical organs exposed to the radiation field.

Although global metabolic changes caused by IR have been identified, which of these could be targeted to confer selective radioresistance is unknown. To globally identify molecular mechanisms by which CD47 blockade selectively confers resistance to the metabolic stress caused by IR, we have performed a metabolomic analysis of Jurkat T cells and a somatic mutant derived from this cell line that specifically lacks CD47 (24). In parallel, metabolic changes in response to irradiation were studied in WT and *cd47*-null mice. These studies demonstrate that CD47 blockade or deficiency broadly prevents detrimental metabolic alterations associated with radiation injury.

Experimental Procedures

Cells—Wild type Jurkat T cells (E6.1, ATCC) and the CD47-deficient (CD47(−)) Jurkat somatic mutant clone JinB8 (24) were maintained at 2–5 $\times$ 10^5 cells per ml in RPMI 1640 medium supplemented with glutamine, penicillin/streptomycin, and 10% FBS (Life Technologies). Cells were maintained in culture for a maximum of 4 weeks.

Irradiation of Cells—Cells were expanded to 5 million cells per sample. Cells were passed into fresh complete media to 1 $\times$ 10^6 cells per ml on the day before irradiation. On the day of irradiation, cells were pooled into 125-cm^2 tissue culture flasks and irradiated using a Precision X-Ray X-Rad 320 (operating at kV/10 mA with a 2-mm aluminum filter; Precision X-Ray, East Haven, CT). The dose rate at 50 cm from the x-ray source was 242 centiGy/minute as determined by multiple thermoluminescent dosimeter readings. Control cells (non-irradiated, t = 0) were handled in the exact same manner with the exception of radiation exposure. At 0, 2, or 8 h after IR exposure, cells were pelleted in 50-ml conical tubes and transferred to pre-cooled 2-ml cryo-vials and immediately frozen on liquid nitrogen. At each time point we sampled both WT and CD47(−) cells in 6 replicates with 5 million cells in each replicate sample. Samples were maintained at ≤−70 °C for 1 week before shipping to Metabolon for analysis.

Mouse Irradiation—WT and *cd47*-null mice (25) extensively back-crossed onto a C57Bl/6J background were obtained from The Jackson Laboratory. All mice were bred in the same vivarium before use to ensure consistent microbiomes. Care and handling of animals was in accordance with protocol LP-012 approved by the Animal Care and Use Committee of the National Cancer Institute. Groups of 12-week-old sex-matched WT and *cd47*-null mice received 7.6 Gy of total body irradiation delivered by a Therapax DXT300 x-ray irradiator (Pantak, Inc., East Haven, CT) using 2.0-mm Al filtration (300 peak kilovoltage) at a dose rate of 2.53 Gy/min. At 24 h post-IR lung tissue was harvested and flash-frozen for metabolomic analysis.

Cell Viability—WT and CD47(−) cells from the same pool of cells destined for metabolomic analysis were plated at a density of 7 $\times$ 10^3 cells/well in 96-well plates. At 24 h after plating, the cells were exposed to a single dose of radiation and allowed to incubate another 72 h at 37 °C. Cell viability was determined by 3-(4,5-dimethylthiazol-2-yl)-5-(3-carboxymethoxyphenyl)-2-(4-sulfophenyl)-2H-tetrazolium (MTS) reduction using the CellTiter 96 Aqueous One Solution cell proliferation assay (Promega G5421) as per the manufacturer's instructions, and absorbance at 490 nm was determined with a 96-well plate based spectrophotometer (Dynatech, Alexandria, VA).

Gene Expression Studies—At the indicated times after irradiation, RNA was extracted using TRIzol (Invitrogen) according to the manufacturer's protocol. cDNA was synthesized from 1–5 μg of total RNA using Superscript first strand RT-PCR reagents (Invitrogen) according to the manufacturer's protocol. Quantitative real-time-PCR was then performed using the SYBR Green kit (Thermo) using specific gene primer sets.

Metabolite Analysis—Metabolomic profiling analysis was performed by Metabolon as previously described (26, 27). Each sample was accessioned into the Metabolon LIMS system and was assigned by the LIMS, a unique identifier that was associated with the original source identifier only. This identifier was used to track all sample handling, tasks, results, etc. The samples (and all derived aliquots) were tracked by the LIMS system. All portions of any sample were automatically assigned their own unique identifiers by the LIMS when a new task is created; the relationship of these samples is also tracked. All samples were maintained at −80 °C until processed.

Sample Preparation—Samples were prepared using the automated MicroLab STAR® system from Hamilton Company. A recovery standard was added before the first step in the extraction process for quality control purposes. Sample preparation was conducted using aqueous methanol extraction process to remove the protein fraction while allowing maximum recovery of small molecules. The resulting extract was divided into four fractions: one for analysis by ultrahigh performance liquid chromatography/tandem mass spectrometry (UPLC/MS/MS, positive mode), one for UPLC/MS/MS (negative mode), one for gas chromatography/mass spectrometry (GC/MS), and one for backup. Samples were placed briefly on a TurboVap® (Zymark)

to remove the organic solvent. Each sample was then frozen and dried under vacuum. Samples were then prepared for the appropriate instrument, either UPLC/MS/MS or GC/MS.

UPLC/MS/MS—The LC/MS portion of the platform was based on a Waters ACQUITY UPLC and a Thermo-Finnigan linear trap quadrupole mass spectrometer, which consisted of an electrospray ionization source and linear ion-trap mass analyzer. The sample extract was dried then reconstituted in acidic or basic LC-compatible solvents, each of which contained eight or more injection standards at fixed concentrations to ensure injection and chromatographic consistency. One aliquot was analyzed using acidic positive ion optimized conditions and, the other was analyzed using basic negative ion-optimized conditions in two independent injections using separate dedicated columns. Extracts reconstituted in acidic conditions were gradient-eluted using water and methanol containing 0.1% formic acid, whereas the basic extracts, which also used water/methanol, contained 6.5 mM ammonium bicarbonate. The MS analysis alternated between MS and data-dependent MS^2 scans using dynamic exclusion. Raw data files are archived and extracted as described below.

GC/MS—The samples destined for GC/MS analysis were re-dried under vacuum desiccation for a minimum of 24 h before being derivatized under dried nitrogen using bistrimethyl-silyl-triflouroacetamide. The GC column was 5% phenyl, and the temperature ramp was from 40 ° to 300 °C in a 16-min period. Samples were analyzed on a Thermo-Finnigan Trace DSQ fast-scanning single-quadrupole mass spectrometer using electron impact ionization. The instrument was tuned and calibrated for mass resolution and mass accuracy on a daily basis. The information output from the raw data files was automatically extracted as discussed below.

*A*dditional samples were included with each day's analysis for quality control. These samples included extracts of a pool created from a small aliquot of the experimental samples and process blanks. Quality control samples were spaced evenly among the injections, and all experimental samples were randomly distributed throughout the run. A selection of quality control compounds was added to every sample for chromatographic alignment, including those under test. These compounds were carefully chosen so as not to interfere with the measurement of the endogenous compounds.

Data Extraction and Compound Identification—Raw data were extracted, peak-identified, and quality control-processed using Metabolon's hardware and software. These systems are built on a web-service platform utilizing Microsoft's .NET technologies, which run on high performance application servers and fiber-channel storage arrays in clusters to provide active failover and load-balancing. Compounds were identified by comparison to library entries of purified standards or recurrent unknown entities. More than 2400 commercially available purified standard compounds have been acquired and registered into LIMS for distribution to both the LC and GC platforms for determination of their analytical characteristics.

Measurement of Glucose Uptake—Glucose uptake by WT and CD47-defficient Jurkat T cells was measured by using NBDG (2-(*N*-(7-nitrobenz-2-oxa-1,3-diazol-4-yl)amino)-2-deoxyglucose), a fluorescently labeled deoxyglucose analog (Life Technologies). Briefly, cells were left untreated or exposed to a 10 Gy dose of IR. Fluorescent Units were quantified 24 h after treatment ($n = 3$. *, $p < 0.05$).

Measurement of Citrate Synthase Activity—Citrate synthase activity was determined in homogenates prepared from Jurkat cells using a citrate synthase assay kit (CS0720; Sigma). Protein was determined using the bicinchoninic acid assay, and normalized concentration was used to perform the assay. Citrate synthase activity was determined in triplicate based on the formation of 2-nitro-5-thiobenzoic acid at a wavelength of 412 nm at 25 °C on a spectrophotometer. In each well, a 1 μg/μl of sample was added to a reaction medium containing assay buffer (30 mM acetyl coenzyme A and 10 mM 2-nitro-5-thiobenzoic acid). The baseline solution absorbance was recorded, reactions were initiated by the addition of 10 μl of oxaloacetic acid, and the change in absorbance was measured every 20 s for 2 min.

Flow Cytometry—WT and CD47(−) Jurkat T cells were irradiated with 10 Gy, and flow-cytometry analysis was performed 24 h later. Cells were stained with anti-human glucose-transporter-1 (GLUT1) (Thermo Scientific, Rockford, IL) followed by anti-rabbit Alexa Fluor 488 dye (Thermo Scientific). Cells were washed three times and resuspended in Hanks' balanced salt solution at 1×10^6 cells in 1000 μl. Samples then were analyzed on a LSRII (BD Biosciences).

Measurement of GSH and GSSG—WT and CD47(−) Jurkat cells were collected before and at 2, 8, and 24 h after irradiation with 10 Gy or sham treatment using 5 million cells per time point/treatment. Cells were washed twice with PBS and lysed according to the manufacturer's protocol using the glutathione assay kit (Cayman Chemical 703002). GSH and GSSG were quantified using the kit and normalized to the total protein in each sample. The absolute GSH and GSSG concentrations were used to calculate the half-cell potential of the redox couple $2GSH \leftrightarrow GSSG + 2H^+$ using the Nernst equation at pH 7.4 and 25 °C. *Error bars* indicate the S.E. of $n = 3$.

Measurement of NADH/NAD^+ and Total NAD—WT and CD47(−) Jurkat T cells were collected before and at 2, 8, and 24 h after irradiation with 10 Gy or sham treatment using 5 million cells per time point/treatment. Cells were washed twice with PBS and lysed according to the manufacturer's protocol using the NAD/NADH assay kit (Abcam ab65348). NADH and NAD^+ were quantified using the kit and normalized to the total protein in each sample. *Error bars* indicate a S.E. of $n = 2$.

Statistical Analysis—Missing values (if any) are assumed to be below the level of detection. However, biochemicals that were detected in all samples from one or more groups but not in samples from other groups were assumed to be near the lower limit of detection in the groups in which they were not detected. In this case, the lowest detected level of these biochemicals was imputed for samples in which that biochemical was not detected. After log transformation and imputation with minimum observed values for each compound, data were protein-normalized by Bradford assay, and both an ANOVA contrast and two-way ANOVA with random effects were used to identify biochemicals that differed significantly between experimental groups. Pathways were assigned for each metabolite, allowing examination of overrepresented pathways.

Results

CD47 Controls Global Metabolic Resistance to Radiation—WT and CD47(−) Jurkat T cells used for metabolomic analysis were irradiated at 10 Gy and analyzed after 2 or 8 h along with untreated controls. Consistent with our published findings (22), viability of the irradiated WT cells was reduced to 40% at 72 h, but 90% of the irradiated CD47(−) cells remained viable (Fig. 1*A*). As expected, irradiation of WT Jurkat T cells resulted in profound alterations in cellular metabolism (4, 7). Of the 342 named metabolites quantified, 27 were significantly altered at 2 h and 112 at 8 h after irradiation (Table 1). Of these, the majority progressively fell below baseline levels (81% at 2 h and 98% at 8 h, respectively). In contrast, the metabolome of irradiated CD47(−) cells was remarkably stable, with only 6 metabolite levels significantly altered at 2 h and 29 at 8 h. Remarkably, 86% of the metabolites in CD47(−) cells that were altered at 8 h showed increased rather than decreased abundance. Thus, the overall conclusion of this analysis is that CD47(−) cells are globally resistant to the metabolic changes caused by IR. Moreover, the opposing directions of metabolite alterations at 8 h suggest that CD47(−) cells actively compensate for radiation stress by increasing levels of key metabolites.

Globally, CD47(−) cells are also in a distinct basal metabolic state (Table 1). Levels of 94 (27%) of the measured metabolites differed significantly between non-irradiated WT and CD47(−) cells. Of these the majority were lower in CD47(−) cells, but 8 h after irradiation the majority became higher in the CD47(−) cells. ANOVA analysis indicated that the variance for 128 of the metabolites was primarily attributable to CD47 genotype, 23 primarily to time-dependent radiation effects, and 53 to the interaction between CD47 genotype and irradiation. Thus, CD47 expression has major impacts on Jurkat T cell metabolism in the absence and presence of genotoxic stress.

CD47 Regulates Cellular Energetics—Examination of specific metabolic pathways revealed multiple effects of CD47 signaling on cellular energetics under basal conditions and in response to radiation. The major energy currency of cells is glucose, and IR was previously shown to acutely induce cellular glucose uptake at 2–5 h into LS180 colon adenocarcinoma cells by stimulating expression of the transporter GLUT1 and its retention by hexokinase-mediated phosphorylation (28). Because CD47 deficiency elevates c-Myc levels (29) and c-Myc is known to positively regulate glucose uptake (30), we examined uptake of NBDG (Fig. 1*B*). Consistent with their increased c-Myc expression, CD47(−) cells showed elevated basal uptake. NBDG uptake decreased 2 h after irradiation in WT and CD47(−) cells and remained significantly higher in irradiated CD47(−) cells than in irradiated WT and slightly above that of untreated WT cells. The increase in glucose uptake was associated with increased GLUT1 expression in CD47(−) cells after exposure to IR when compared with WT cells (1C).

A metabolic tracing study using 1,2-[^{13}C]glucose determined that ~60% of glucose is metabolized by Jurkat cells via glycolysis to lactate (31). Glycolytic intermediates were generally lower in untreated CD47(−) cells than in WT cells (Fig. 1*D*). Based on the increased uptake of glucose, the lower basal levels of glycolytic intermediates in CD47(−) cells probably indicate less downstream regulation of the glycolytic flux in CD47(−) cells. After irradiation, levels of glycolytic metabolites generally fell in WT cells but were maintained in CD47(−) cells. Consistent with a report that high dose radiation decreased fructose/glucose-1,6-diphosphate, dihydroxyacetone phosphate, and lactate levels in guinea pig myocardium (32), fructose/glucose-1,6-diphosphate, dihydroxyacetone phosphate, pyruvate, and lactate all declined significantly at 8 h after irradiation in WT cells but remained stable in CD47(−) cells. The one exception to this trend was free glucose, which was transiently elevated in WT cells 2 h after irradiation. These results further indicate that metabolism of glucose via glycolysis decreases after irradiation of WT cells but persists in CD47(−) cells.

Although basal intracellular lactate levels did not differ significantly between WT and CD47(−) cells, assessment of extracellular acidification 24 h after irradiation further indicated that CD47(−) cells maintain a higher flux of glucose metabolism to lactate (Fig. 1*E*). In contrast to the selective fall in intracellular lactate in irradiated WT cells, extracellular acidification was not significantly altered by irradiation in either cell line.

CD47 Regulation of the Pentose Phosphate Pathway and Nucleotide Biosynthesis—Based on isotopic metabolic tracing, the pentose phosphate pathway (PPP) contributes only ~3% of lactate production in Jurkat cells (31), but this pathway is a major source of intermediates for *de novo* nucleotide biosynthesis and provides cellular NADPH required for handling oxidative stress and repairing damage caused by radiation. Basal 6-phosphogluconate was higher in CD47(−) cells. A lower basal flux through the PPP for CD47(−) cells was suggested by lower levels of ribose and ribulose. Remarkably, IR induced opposing changes in the PPP in WT and CD47(−) cells (Fig. 2). Levels of 6-phosphogluconate rapidly increased in irradiated WT cells but fell to WT levels in CD47(−) cells. Taken together these data indicate that radiation stress in WT but not CD47(−) cells is associated with a shift from glycolysis to the PPP for metabolism of glucose. Thus, WT cells progressively lose their capacity to maintain glycolysis and only transiently increase flux through the PPP after irradiation, but these pathways remain relatively stable in irradiated CD47(−) cells.

Ribose 5-phosphate derived from the PPP is required for *de novo* nucleotide biosynthesis. Inosine 5-monophosphate is a key intermediate in purine nucleotide biosynthesis. Untreated WT and CD47(−) cells had comparable basal levels of inosine 5′-monophosphate (Fig. 3*A*). After irradiation, levels fell significantly in WT cells but were elevated in CD47(−) cells. Similar differences between WT and CD47(−) cells were seen in levels of adenine and guanine nucleotides that derive from inosine monophosphate. Levels of adenylsuccinate, AMP, ADP, deoxy-ADP, and GMP fell progressively after irradiation in WT cells but remained stable in CD47(−) cells (Fig. 3*A*). Pyrimidine nucleotide biosynthesis in irradiated cells was similarly sensitive to CD47, with uridine 5′-monophosphate and downstream metabolites falling in irradiated WT cells but not in CD47(−) cells (Fig. 3*B*). Thus, CD47 coordinately regulates nucleotide biosynthesis required to repair DNA damage caused by IR, and CD47 deficiency preserves nucleotide biosynthetic capacity in irradiated cells.

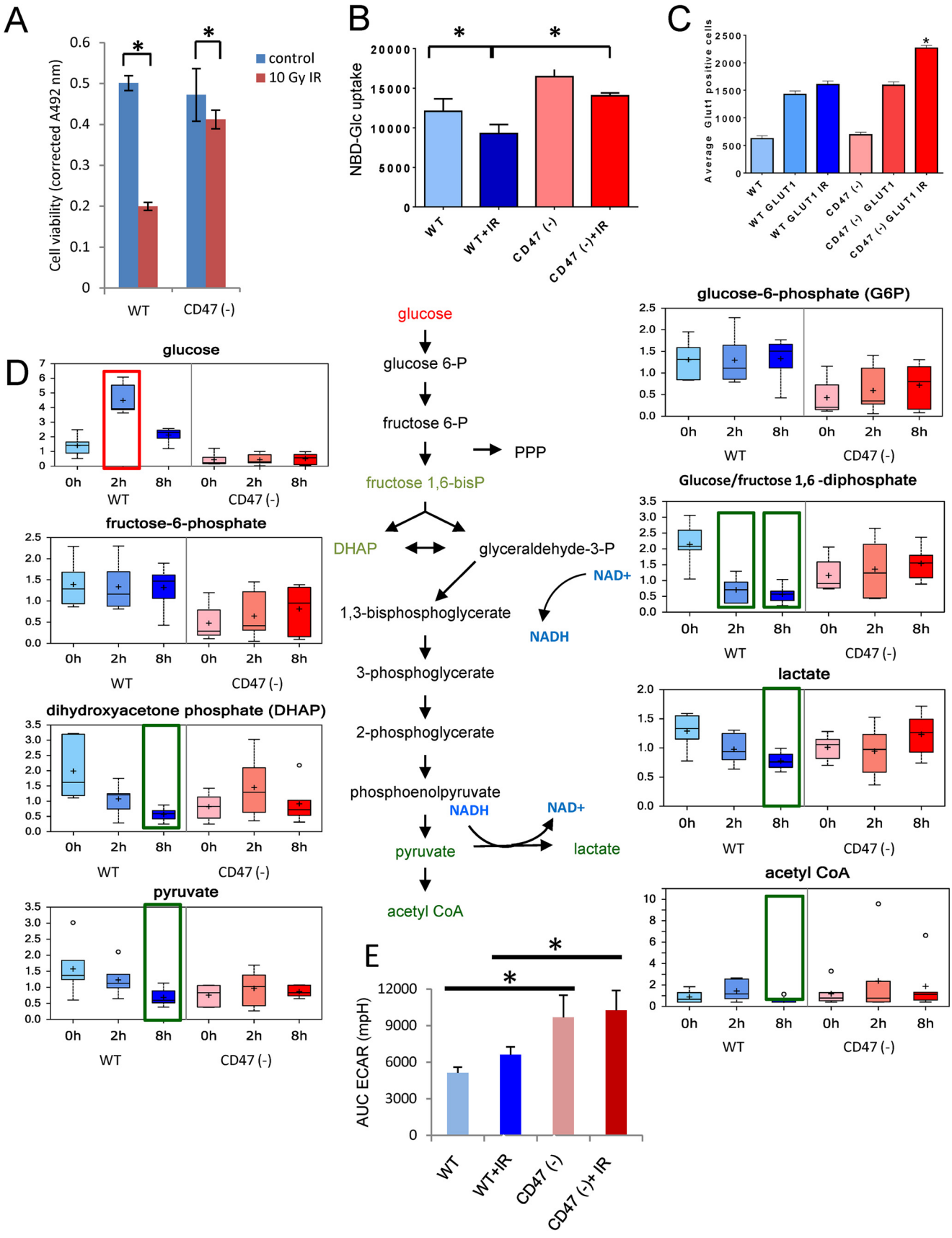
A
Cell viability (corrected A492 nm)
control
10 Gy IR
WT
CD47 (-)
B
NBD-Glc uptake
WT
WT+IR
CD47 (-)
CD47 (-)+IR
C
Average Glut1 positive cells
WT
WT GLUT1
WT GLUT1 IR
CD47 (-)
CD47 (-) GLUT1
CD47 (-) GLUT1 IR
D
glucose
fructose-6-phosphate
dihydroxyacetone phosphate (DHAP)
pyruvate
glucose-6-phosphate (G6P)
Glucose/fructose 1,6 -diphosphate
lactate
acetyl CoA
0h
2h
8h
WT
CD47 (-)
glucose
glucose 6-P
fructose 6-P
PPP
fructose 1,6-bisP
DHAP
glyceraldehyde-3-P
NAD+
NADH
1,3-bisphosphoglycerate
3-phosphoglycerate
2-phosphoglycerate
phosphoenolpyruvate
NADH
NAD+
pyruvate
lactate
acetyl CoA
E
AUC ECAR (mpH)
WT
WT+IR
CD47 (-)
CD47 (-)+IR

TABLE 1

Summary statistics of global metabolic responses to ionizing radiation in WT and CD47-deficient Jurkat T cells

Top panel; Numbers of named metabolites that were significantly up- or down regulated (↑ | ↓) based on ANOVA contrasts for the indicated comparisons. Bottom panel; Numbers of altered metabolites significantly associated with genotype, time, or the interaction between genotype and time variables based on two-way ANOVA.

	CD47-deficient/WT			Comparisons to Baseline			
				WT		CD47-deficient	
	0h	2h	8h	2h / 0h	8h / 0h	2h / 0h	8h / 0h
Total biochemicals $p \leq 0.05$	94	88	105	27	112	6	29
Biochemicals (↑|↓)	13|81	33|55	83|22	5|22	2|110	0|6	25|4

Two-Way ANOVA	Genotype Main Effect	Time Main Effect	Genotype:Time Interaction
Total biochemicals $p \leq 0.05$	128	23	53
Total biochemicals $0.05 < p < 0.10$	29	21	42

Several additional metabolites involved in DNA damage repair showed CD47-dependent responses to irradiation. 5-Methyltetrahydrofolate is required for thymidine biosynthesis, and folate restriction is known to increase DNA damage caused by IR (33). After IR exposure, 5-methyltetrahydrofolate levels declined at 2 and 8 h in WT cells but remained stable in CD47(−) cells (Fig. 3*B*). Pyrophosphate (PP_i) is released, as nucleotides are incorporated into DNA, which is associated with radiation-induced DNA damage *in vivo* (34). PP_i levels were diminished by 8 h in WT cells, but no significant differences were observed in irradiated CD47-deficient cells (supplemental Table 1). Lower levels of PP_i in WT cells further indicate a decreased capacity for DNA synthesis/repair after radiation exposure. Biotin serves as a covalently bound coenzyme in select carboxylases and is also attached to histones. In this capacity, biotin is required for the prevention of DNA damage (35). Biotin levels significantly declined in WT cells by 8 h but only transiently decreased in CD47(−) cells (Supplemental Table 1).

CD47 Regulation of the Krebs Cycle—Tricarboxylic acid (TCA) cycle metabolites were strongly regulated by CD47 expression. Most TCA intermediates progressively fell in irradiated WT cells but not in irradiated CD47(−) cells (Fig. 4). Substrates feeding into the TCA cycle and intermediary metabolites in this cycle did not differ basally between WT and CD47(−) cells. However, levels of the citrate synthase products citrate and 2-methyl citrate, the latter derived from catabolism of some aliphatic amino acids and odd chain fatty acids, were significantly lower in CD47(−) cells. Lower levels of propionyl carnitine in CD47(−) cells were consistent with the lower 2-methylcitrate level (supplemental Table 1), suggesting decreased basal lipid and/or aliphatic amino acid catabolism in the absence of CD47.

Because levels of the citrate synthase substrate acetyl-CoA and the TCA intermediates succinate, fumarate, and malate were not lower in irradiated CD47(−) cells, we considered that citrate synthase may be negatively regulated by CD47 signaling, thereby preventing accumulation of citrate and 2-methylcitrate. Consistent with this hypothesis, basal levels of citrate synthase mRNA and enzymatic activity were lower in CD47(−) cells (Fig. 4, *B* and *C*). IR resulted in further decreases in citrate levels in CD47-deficient cells but not in WT cells. Citrate synthase mRNA levels progressively decreased in irradiated WT cells, but levels were elevated 6-fold and 10-fold at 8 and 24 h, respectively, in irradiated CD47(−) cells. Consistent with the low citrate levels at 2 and 8 h and the late induction of its mRNA, citrate synthase activity in CD47(−) cells remained low at 2 and 8 h but increased 24 h after exposure to IR. This suggests that citrate synthase activity in irradiated CD47(−) cells is regulated at the protein level, whereas the elevated citrate synthase mRNA in irradiated CD47(−) cells may result from loss of catabolite repression as previously reported for citrate synthase in yeast (36).

Blockage of the TCA cycle at citrate synthase may also explain the remarkable elevation of acetylated peptide metabolites in CD47(−) cells (Fig. 5). In brain, acetylated peptides derive from redirection of the citrate synthase substrates via aspartyl aminotransferase and aspartyl *N*-acetyltransferase to synthesize *N*-acetyl aspartate (*NAA*), which was elevated ~5-fold in CD47(−) cells relative to WT (Fig. 5*A*). *N*-Acetyl aspartate can be further metabolized to *N*-acetyl-aspartyl-glutamate, and this dipeptide was similarly elevated in CD47(−) cells. Recent studies have revealed that this pathway occurs outside the CNS in pancreatic cancer (37), and cells bearing isocitrate dehydrogenase mutations showed a corresponding depletion of these two acetylated peptides (26). Thus, we propose that the absence of CD47 redirects carbon flux through the TCA cycle and acetyl-CoA toward synthesis of acetylated peptide metabolites.

N-Acetyl-aspartyl-glutamate is degraded extracellularly by the membrane-bound dipeptidyl peptidase encoded by *NAALAD2* (38). NAALAD2 mRNA levels were induced ~3-fold 2 h after irradiation in WT cells but >10-fold in CD47(−) cells ($p < 0.05$; Fig. 5*B*). Thus, CD47(−) cells may have increased capacities to both synthesize and extracellularly degrade acetylated peptides.

Preservation of Mitochondrial Function in the Absence of CD47—Consistent with the elevated mitochondrial numbers and function reported in some tissues of *cd47*-null mice (39), CD47(−) Jurkat cells had more mitochondrial mass than WT cells based on Mitotracker staining (Fig. 6*A*). mRNA levels for

FIGURE 1. **CD47 regulates glucose uptake and glycolysis.** *A*, MTS viability assay for WT and CD47(−) Jurkat T cells before and after irradiation at 10 Gy. *B*, uptake of NBDG was measured 24 h after irradiation at 10 Gy. *C*, GLUT1 expression assessed by flow cytometry. *D*, glycolytic metabolites were quantified before and 2 and 8 h after irradiation of WT and CD47(−) cells. *E*, extracellular acidification rate (*ECAR*) was used to assess glycolytic flux to lactate in control and irradiated cells (mean ± S.D. $n = 3–4$; *, denotes $p < .01$). *AUC*, area under the curve. Significant up- or down-regulation of individual metabolites relative to the respective basal levels ($p < 0.05$) is indicated by *red* and *green boxes*, respectively. For the box plots in all figures: *center horizontal line* = median value; + = mean value; box height = limits of upper and lower quartiles, *whiskers* = max and min of distribution; ○ = extreme data point; $n = 6$.

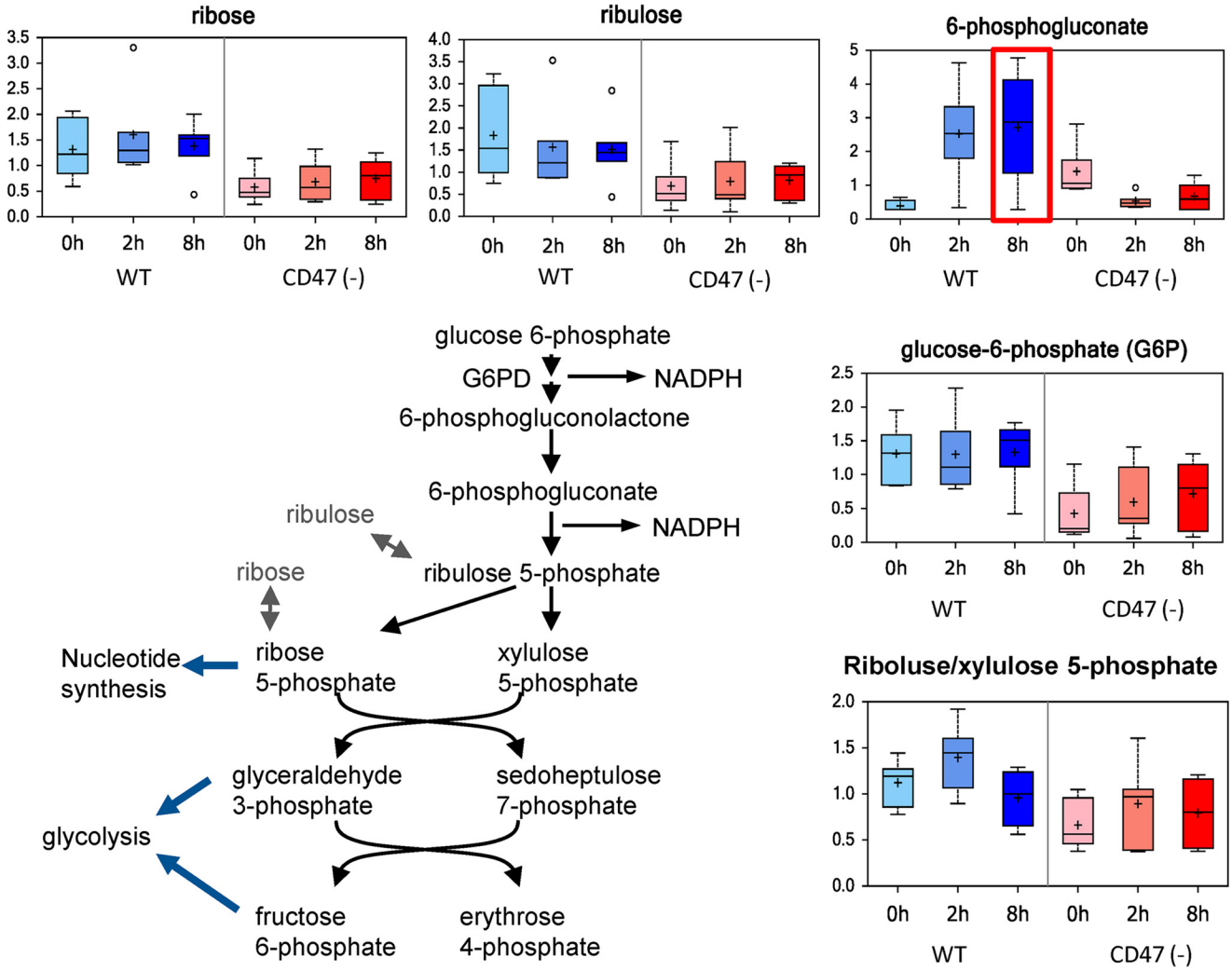

FIGURE 2. **CD47 regulates the pentose phosphate pathway.** The indicated metabolites in the pentose phosphate pathway were quantified before and 2 and 8 h after irradiation of WT and CD47(−) Jurkat cells.

the mitochondrially encoded cytochrome C oxidase subunit-1 (*MTCO1*) were also higher in CD47(−) cells (Fig. 6*B*). At 24 h after irradiation, we observed a further increase in mitochondrially encoded cytochrome C oxidase subunit-1 mRNA in irradiated CD47(−) cells but no significant change in WT cells.

Basal and radiation-induced changes in mitochondrial energy metabolism were validated by assessing cellular oxygen consumption. The basal oxygen consumption rate (OCR) was elevated in untreated CD47(−) cells relative to WT cells (Fig. 6, *C* and *E*). Basal OCR was elevated in both cell lines after irradiation but remained higher in the CD47(−) cells. The irradiated CD47-deficicent cells also exhibited a greater spare respiratory capacity as indicated by the marked increase in OCR when irradiated CD47(−) cells were treated with the electron transport accelerator carbonyl cyanide-4-(trifluoromethoxy)phenylhydrazone (*FCCP*; Fig. 6*C*). WT cells treated with an antisense morpholino to decrease CD47 expression had increased spare respiratory capacity (defined by the difference in basal and carbonyl cyanide-4-(trifluoromethoxy)phenylhydrazone-treated OCR) after irradiation, confirming that CD47 regulates mitochondrial respiration (Fig. 6*D*).

Non-mitochondrial oxygen consumption was minimal in Jurkat cells under all conditions. The increased mitochondrial flux in CD47(−) cells implies that these cells maintain a more favorable NADH/NAD^+ ratio. We could not determine absolute NADH/NAD^+ ratios from the metabolomic data, but independent enzymatic measurement of NAD^+ and NADH concentrations confirmed a more favorable basal NADH/NAD^+ ratio in CD47(−) cells (Fig. 6*H*). The higher NADH/NAD^+ ratio in CD47(−) cells was maintained after irradiation. In addition, the total NAD level is significantly lower in the CD47(−) cells (19%; $p < 0.01$; Fig. 6*I*) at 24 h post IR exposure *versus* pre-exposure. The decrease in total NAD levels at 24 h post exposure in the CD47(−) cells could be due to the increased demand for DNA repair and were thereby consistent with ribose 5-phosphate data discussed above. Total NAD levels normalized to total protein were consistently lower in CD47(−) cells than WT. However, this may reflect increased per cell protein levels induced by c-Myc in CD47(−) cells (29).

PGC1α is a key transcriptional coactivator that regulates mitochondrial homeostasis and coordinates lipid oxidation with TCA cycle flux. Activation of PGC1α can protect tissues

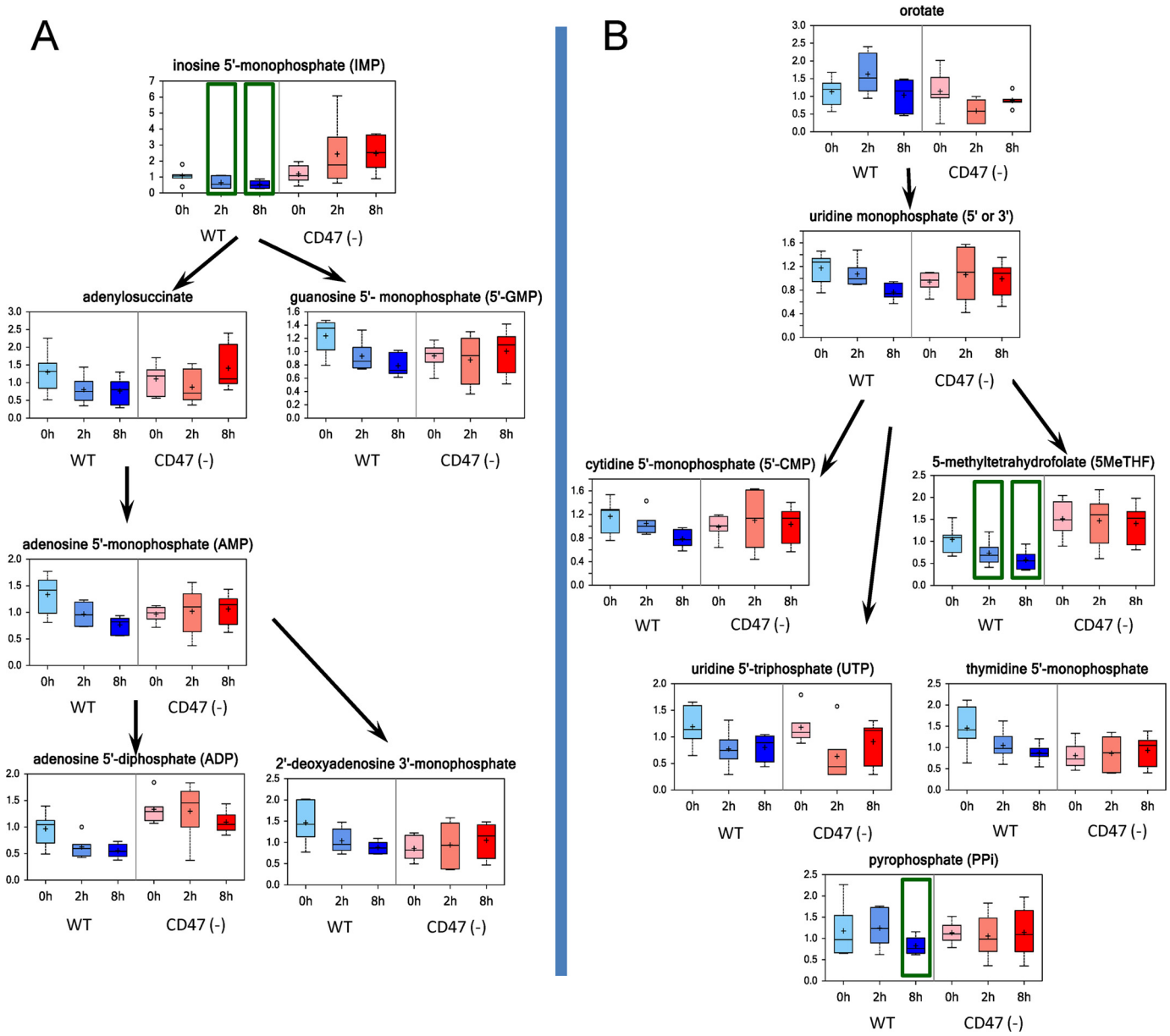

FIGURE 3. **CD47 deficiency protects nucleotide biosynthetic pathways and enhances repair of radiation-induced DNA damage.** A, intermediates in purine nucleotide biosynthesis were quantified before and 2 and 8 h after irradiation of WT and CD47(−) Jurkat cells. *B*, intermediates in pyrimidine nucleotide biosynthesis were quantified before and 2 and 8 h after irradiation of WT and CD47(−) cells.

by limiting oxidative stress (40, 41). Radiation induced increases in PGC1α mRNA levels in both cell lines, but levels were higher in the CD47(−) cells 24 h post IR (Fig. 6*F*). Glutathione peroxidase-1 (Gpx1) is a known target of PGC1α and was also elevated selectively in irradiated CD47(−) cells (Fig. 6*G*).

CD47 Regulates Labile Methyl Group Homeostasis—Creatine is a critical element of cellular energetics in some tissues by providing a reservoir for the high energy phosphate donor phosphocreatine (42). Creatine biosynthesis also accounts for a majority of the metabolic utilization of labile methyl groups and thus is an indicator of the availability of methyl donors for other biosynthetic and epigenetic regulatory functions. The decreased levels of creatine and its non-enzymatic catabolite creatinine in irradiated WT cells at 8 h are consistent with the decreased creatine levels that were reported in irradiated rat limbs (43) (Fig. 7*A*). Increased urinary excretion of creatine and its catabolite creatinine are biomarkers of whole body irradiation in rats (44), and creatine was identified as a urinary radiation biomarker in a nonhuman primate (11). Notably, baseline creatine levels were much higher in CD47(−) cells and persisted after irradiation (Fig. 7*A*). This may provide cytoprotection to CD47(−) cells given that exogenous creatine was shown to protect keratinocytes from free radical damage caused by UV irradiation (45).

The mechanism by which CD47 limits creatine levels in WT cells remains to be determined, but levels of its metabolic precursors cannot explain the marked elevation in CD47(−) cells. Levels of the precursors arginine and glycine were moderately lower in untreated CD47(−) cells (Fig. 7*A* and supplemental

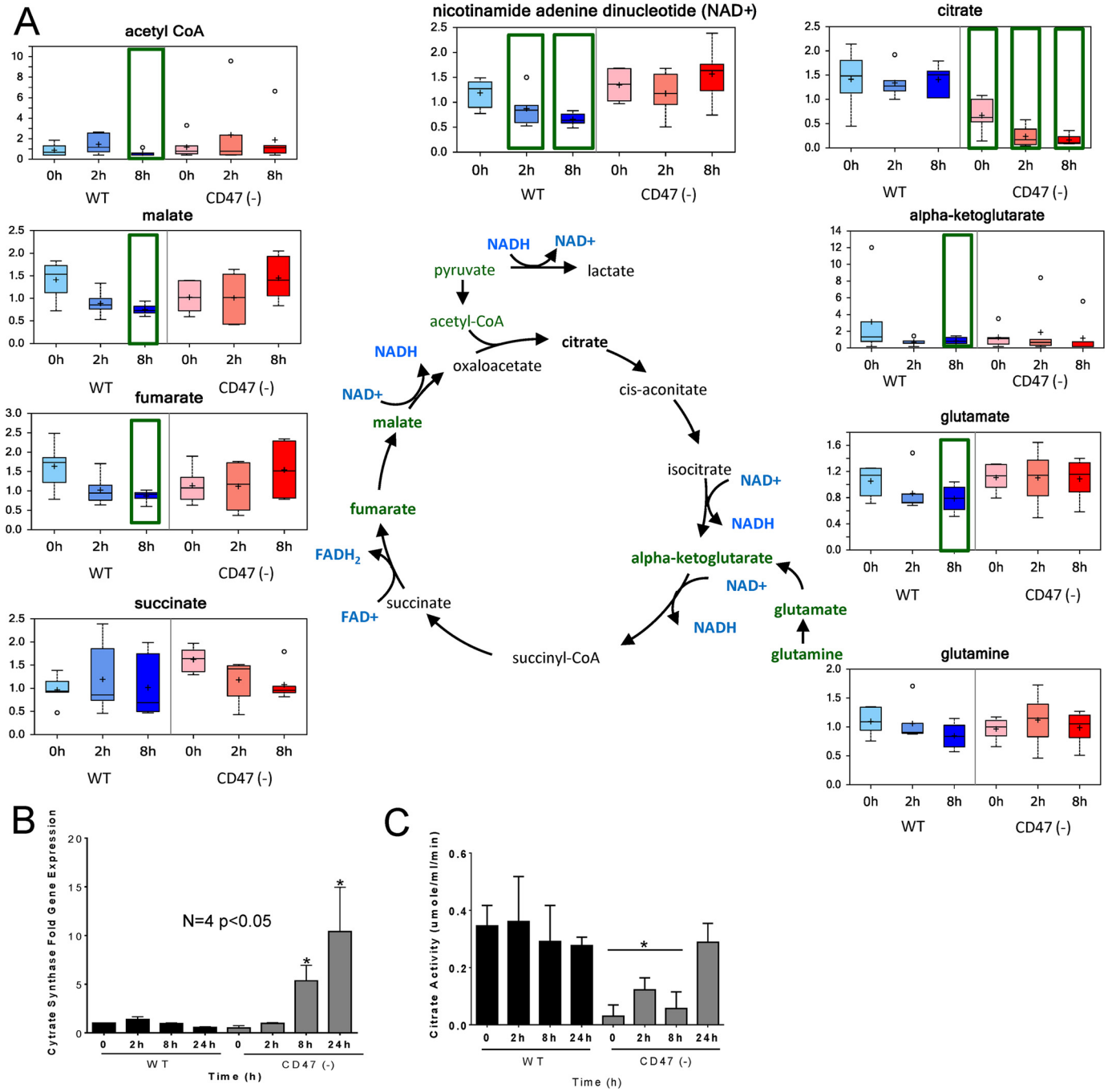

FIGURE 4. **CD47 deficiency prevents the loss of tricarboxylic acid flux caused by IR.** *A*, metabolites in the tricarboxylic acid pathway were quantified before and 2 and 8 h after irradiation of WT and CD47(−) Jurkat cells. *B*, citrate synthase mRNA levels were assessed before and 2, 8, or 24 h after irradiation of WT and CD47(−) cells. *C*, citrate synthase enzyme levels were evaluated at 0, 2, 8, and 24 h post-radiation (mean ± S.D., $n = 3$, *, $p < 0.05$).

Table 1). Biosynthesis of creatine also requires the methyl donor *S*-adenosylmethionine, and basal *S*-adenosylmethionine levels were notably higher in CD47(−) cells (Fig. 7*A*).

The limiting step in creatine biosynthesis is catalyzed by glycine amidinotransferase (GATM). GATM is highly regulated at the level of its gene expression and enzymatic activity. Basal levels of GATM mRNA were similar in WT and CD47(−) cells, but their responses to radiation diverged (Fig. 7*B*). GATM mRNA in WT cells briefly rose at 2 h after irradiation but fell at later time points. Conversely, GATM mRNA levels in CD47(−) cells initially declined but were markedly elevated at 8 and 24 h. Thus, differential CD47-dependent regulation of GATM mRNA may account for the preservation of creatine biosynthesis in irradiated CD47(−) cells, but additional levels of regulation are needed to explain the basal regulation of creatine levels by CD47.

Preservation of labile methyl group availability in irradiated CD47(−) cells is supported by levels of several additional metabolites. 5-Methyl tetrahydrofolate is a critical methyl donor for thymidine biosynthesis, and CD47(−) cells exhibited higher basal 5-Me-THF and selective preservation of these levels after irradiation (Fig. 3*B*). Methyl groups are also required

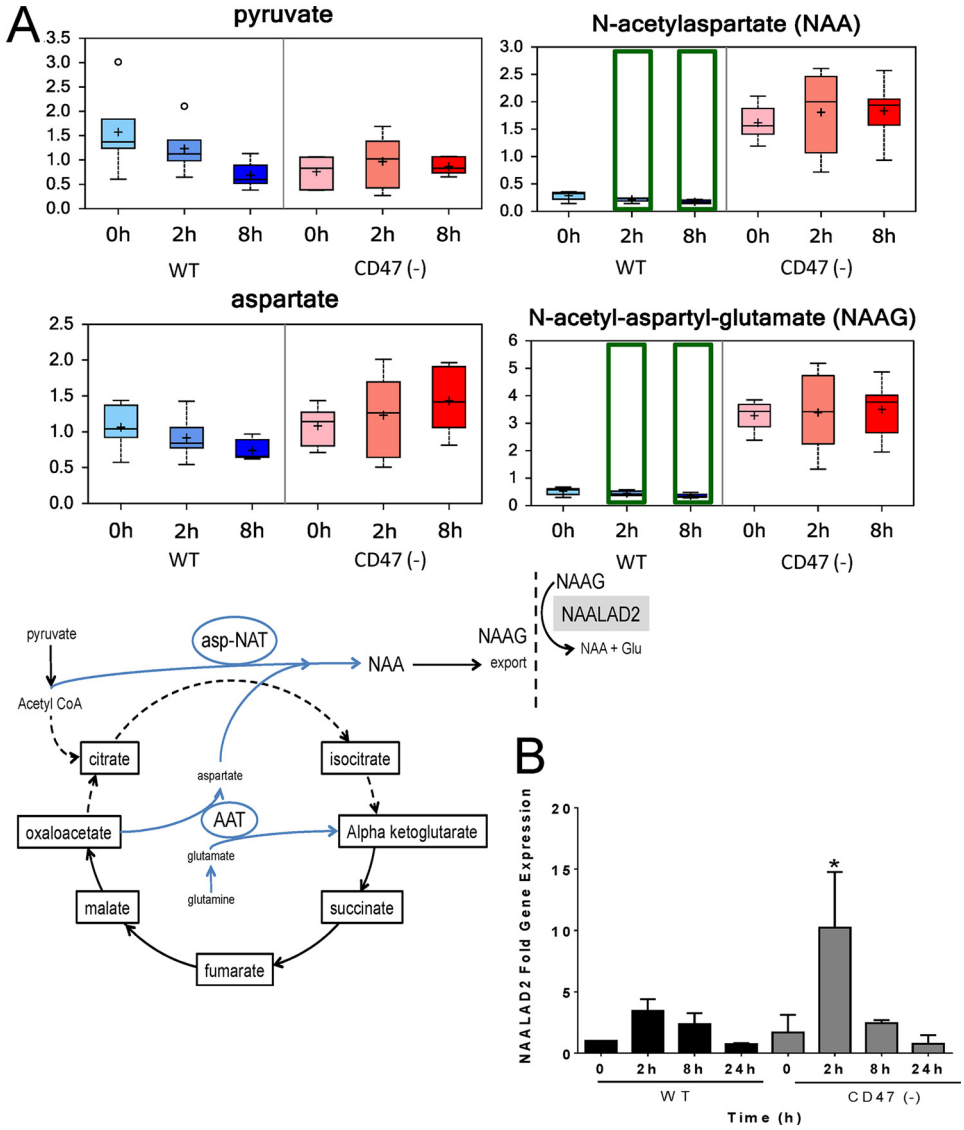

FIGURE 5. **CD47 deficiency redirects basal Krebs cycle metabolism to bypass citrate.** *A*, metabolites involved in shunting of oxaloacetate via aspartyl *N*-acetyltransferase (*asp-NAT*) leading to synthesis of *N*-acetyl-aspartate (*NAA*) and *N*-acetyl-aspartyl-glutamate (*NAAG*) were assessed before and at 2 and 8 h after irradiation. *N*-Acetyl-aspartyl-glutamate released from cells is converted to *N*-acetyl-aspartate and glutamate by *N*-acetylated α-linked acidic dipeptidase-2 (*NAALAD2*). *B*, NAALAD2 mRNA levels were assessed by quantitative RT-PCR at 0, 2, 8, and 24 h after irradiation. *, $p < 0.05$.

for biosynthesis of the mitochondrial lipid carrier carnitine, and levels of carnitine and several acyl carnitines fell after irradiation in WT but not in CD47(−) cells (Fig. 7*C*). Finally, methyl groups are required for biosynthesis of choline phospholipids. Choline levels were significantly lower in WT cells at 2 and 8 h after irradiation but were not affected by irradiation in CD47(−) cells (supplemental Table 1). The precursor for choline phospholipid biosynthesis CDP-choline was corresponding decreased at 8 h in CD47(−) cells but not in WT cells (supplemental Table 1). Comparison of 1-acylglycerophosphocholine and 1-acyglycerophosphoethanolamine intermediates indicated that biosynthesis of choline, but not ethanolamine phospholipids, was enhanced after irradiation of CD47(−) cells, whereas levels of all these lipid intermediates fell after irradiation in WT cells (Fig. 7*D*). Methyl groups can also be recovered from choline by oxidation to betaine, which can transfer a methyl group via betaine homocysteine methyltransferase, ultimately yielding sarcosine (46). Betaine and sarcosine levels fell progressively in irradiated WT cells but remained stable in irradiated CD47(−) cells (supplemental Table 1). Taken together, these data indicate a global enhancement of labile methyl group homeostasis under stress in the absence of CD47 *versus* global loss of transmethylation and methyl neogenesis in irradiated WT cells.

CD47 Limits Oxidative Stress Responses—The glutathione and glyoxalase pathways are critical for cellular redox homeostasis, and previous metabolomics studies documented that these pathways are compromised by exposure of cells to IR (4, 7). Levels of oxidized and reduced glutathione fell progressively as expected in irradiated WT cells (Fig. 8*A*). The half-cell potential of the glutathione redox couple is an informative measure of cell health and biological status (47). The measured potential for the WT and CD47(−) non-irradiated cells (−215 and −200 mV) was slightly lower than that previously reported for WT Jurkat cells (47). This may reflect adventitious oxidation of GSH during sample handling. The data show that

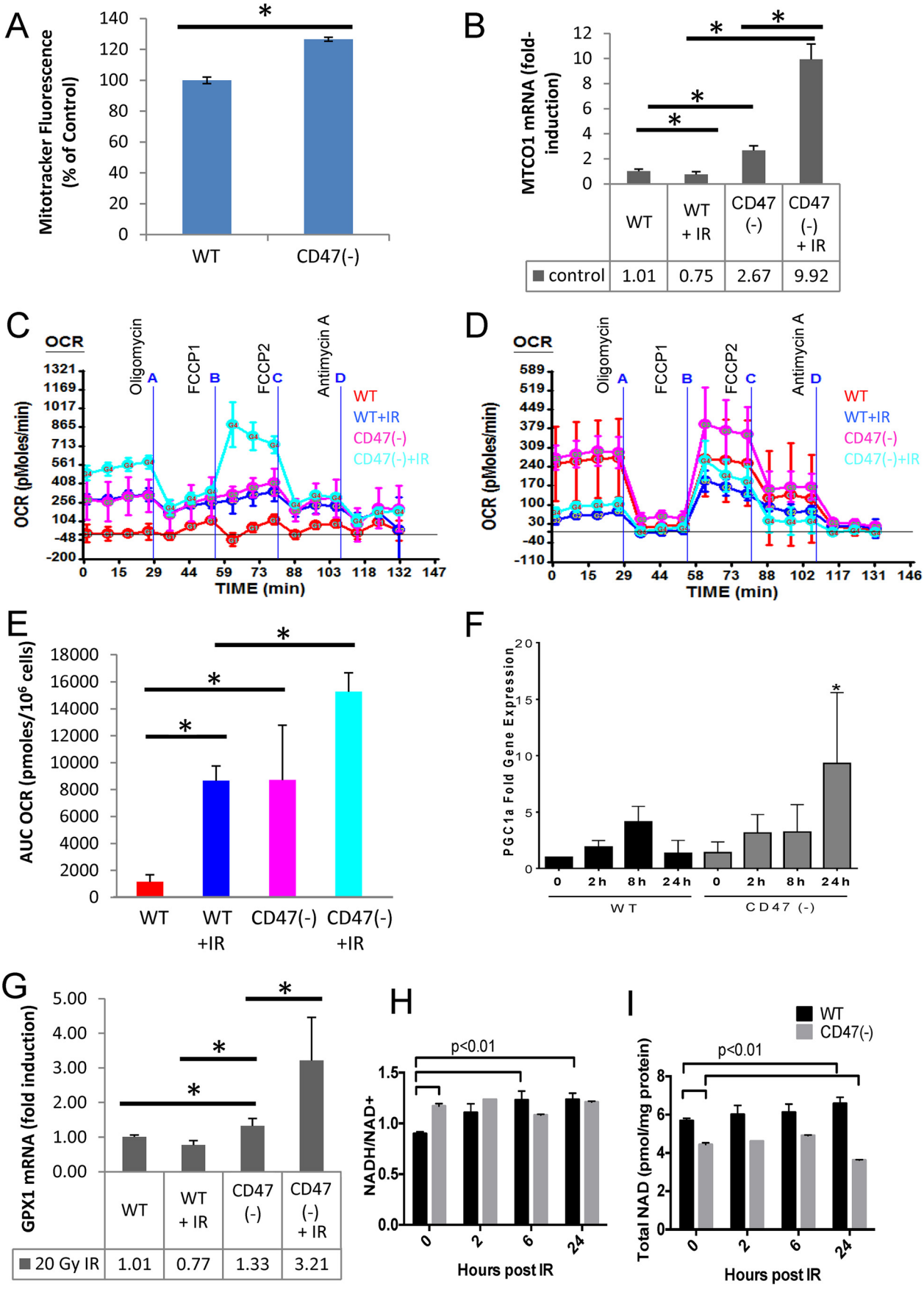
A
Mitotracker Fluorescence (% of Control)
140
120
100
80
60
40
20
0
*
WT
CD47(-)
B
MTCO1 mRNA (fold-induction)
12
10
8
6
4
2
0
*
*
*
WT
WT + IR
CD47 (-)
CD47 (-) + IR
control
1.01
0.75
2.67
9.92
C
OCR
OCR (pMoles/min)
1321
1169
1017
865
713
561
408
256
104
-48
-200
Oligomycin
FCCP1
FCCP2
Antimycin A
A
B
C
D
WT
WT+IR
CD47(-)
CD47(-)+IR
0 15 29 44 59 73 88 103 118 132 147
TIME (min)
D
OCR
OCR (pMoles/min)
589
519
449
379
309
240
170
100
30
-40
-110
Oligomycin
FCCP1
FCCP2
Antimycin A
A
B
C
D
WT
WT+IR
CD47(-)
CD47(-)+IR
0 15 29 44 58 73 88 102 117 131 146
TIME (min)
E
AUC OCR (pmoles/10⁶ cells)
18000
16000
14000
12000
10000
8000
6000
4000
2000
0
*
*
*
WT
WT +IR
CD47(-)
CD47(-) +IR
F
PGC1a Fold Gene Expression
20
15
10
5
0
*
0
2h
8h
24h
0
2h
8h
24h
WT
CD47 (-)
G
GPX1 mRNA (fold induction)
5.00
4.00
3.00
2.00
1.00
0.00
*
*
*
WT
WT + IR
CD47 (-)
CD47 (-) + IR
20 Gy IR
1.01
0.77
1.33
3.21
H
NADH/NAD+
1.5
1.0
0.5
0.0
p<0.01
0
2
6
24
Hours post IR
I
WT
CD47(-)
Total NAD (pmol/mg protein)
8
6
4
2
0
p<0.01
0
2
6
24
Hours post IR

although the E_{GSH} slightly decreased in irradiated WT cells, the E_{GSH} in CD47(−) cells dramatically increased at 2 h and returned to basal levels, exceeding that of the WT cells at 2 and 8 h (Fig. 8*B*). Consistent with the glutathione data, assessment of total free thiol concentrations in cell lysates using Ellman's reagent showed lower basal levels in CD47(−) cells and an initial decrease at 2 h in irradiated WT cells (Fig. 8*C*). Loss of glutathione in the irradiated WT cells may result in part from the observed suppression of glycolysis (48). Metabolites involved in glutathione biosynthesis including cystathionine, glutamate, γ-glutamylcysteine, and 5-oxoproline fell progressively after irradiation in WT cells, but none of these metabolite levels fell in the CD47(−) cells, and γ-glutamylcysteine levels were elevated above baseline at 8 h (Fig. 8*A*). The latter is the immediate precursor of glutathione, indicating more capacity for biosynthetic replenishment of glutathione after irradiation of the CD47(−) cells. Methylglyoxal is a toxic metabolite produced through cellular responses to radiation-induced redox stress. Glutathione is required for its metabolism to lactate via *S*-lactoylglutathione and glyoxalase I. Glyoxalase I and II are rapidly induced in response to IR (49). Consistent with the loss of glutathione homeostasis in irradiated WT cells, levels of S-lactoylglutathione fell dramatically a 2 and 8 h in WT cells (Fig. 8*D*). This was not observed in CD47(−) cells where *S*-lactoylglutathione levels tended to increase after irradiation. Taken together, these results indicate that irradiated cells maintain a greater capacity to handle redox stress in the absence of CD47.

Improved Metabolic Regulation in Irradiated cd47-null Mouse Tissues—To validate the conclusions from our *in vitro* studies, we exposed WT and *cd47*-null mice to an LD_{70} dose of total body IR and collected the lungs 24 h post-exposure. We selected lungs as this organ is very sensitive to IR and is protected in the *cd47*-null cells by activation of autophagy (22). Consistent with the improved global metabolic stability of irradiated CD47(−) cells, fewer of the 377 identified metabolites were significantly altered after 24 h in lung tissue of irradiated *cd47*-null mice than in lungs from irradiated WT mice (14 and 19%, respectively Fig. 9*A*). Focusing on glucose metabolism, we observed a similar selective enhancement of the PPP in irradiated *cd47*-null lungs (Fig. 9*B*). Glucose levels were reduced 24 h after IR in both WT and *cd47*-null lungs. Lactate was also lowered 24 h after IR in both groups, indicating decreased glycolytic flux independent of CD47. Consistent with the *in vitro* data, basal glucose 6-phosphate and fructose 6-phosphate levels trended lower in *cd47*-null lung tissue. However, glucose 6-phosphate and fructose 6-phosphate accumulated only in irradiated *cd47*-null lung tissue. As found *in vitro*, the increased accumulation of ribose 5-phosphate and sedoheptulose 7-phosphate indicate that *cd47*-null mice preferentially activate the PPP after exposure to IR. Moreover, citrate levels were reduced in irradiated tissue from WT *versus cd47*-null mice. Additionally, malate was reduced in irradiated WT but increased in *cd47*-null tissue, indicating a similar regulation of the TCA cycle *in vivo* as *in vitro*. Taken together these data indicate a similar reprogramming of energy metabolism that enables *cd47*-null tissue to overcome damage caused by IR.

Discussion

These studies identify several novel mechanisms by which CD47 limits the capacity of cells and tissues to survive and recover from damage caused by IR. Whereas mammalian cells normally initiate cell death responses when faced with multiple double-strand breaks in their genomic DNA, CD47(−) cells mount sustained energetic and DNA repair responses that enable them to repair the damage and continue growth. A global analysis of metabolites indicated that CD47 controls vital cellular subsystems necessary for survival of IR injury including cellular energetics, redox balance, and cellular repair pathways. Thus, CD47 serves as a gatekeeper through which thrombospondin-1 in the extracellular environment limits the ability of cells to initiate cell repairs in the face of extensive DNA damage.

CD47 ligation induces programmed cell death in specific cell types (50), which may serve a protective function by triggering death of cells damaged by exposure to IR. Selective removal of damaged cells reduces the risk of malignant transformation caused by IR. However, in the face of a lethal dose of whole body radiation, this response can be counterproductive by preventing engagement of cellular repair processes. We have shown that temporary suppression of CD47 levels improves the survival of mice subjected to lethal irradiation by preserving the function of critical radiosensitive tissues in the bone marrow and gastrointestinal tract (21). Some of the protective cellular metabolic responses observed here may be consequences of known CD47 signaling targets that have been associated with radioresistance including enhanced autophagy, nitric oxide signaling, and c-Myc (18, 21, 22, 29, 50).

Autophagy is necessary for the ability of CD47 blockade to confer radioprotection in Jurkat cells (22) and a major regulator of cell metabolism (51). CD47 increases LC3 lipidation and negatively regulates basal expression of sequestosome-1 (p62/SQSTM1) in Jurkat T cells (22). In addition to its role in autophagy, p62 interacts with p38 MAP kinase and positively regulates mitochondrial metabolism (52). Thus, the lower expression of p62 in CD47(−) cells may explain some of the decreases in mitochondrial metabolites in these cells.

Thrombospondin-1 and CD47 are negative regulators of mitochondrial biogenesis in mice (39), and CD47(−) Jurkat cells correspondingly have more mitochondrial mass than WT cells. Skeletal muscle of *cd47*-null mice has increased expres-

FIGURE 6. **CD47 deficiency enhances mitochondrial function and gene expression.** *A*, relative mitochondrial mass in WT and CD47(−) Jurkat cells was assessed by staining with Mitotracker Green mean ± S.D. $n = 3$; * denotes $p < 0.01$. *B*, Mitochondrial cytochrome-c oxidase-1 (*MTCO1*) mRNA levels were assessed by quantitative RT-PCR after irradiation of WT and CD47(−) cells. *C*, OCR were assessed using an XF24 analyzer in control and irradiated WT and CD47(−) cells. *D*, blockade of CD47 regulates oxygen consumption rate in WT cells. OCRs were assessed using an XF24 analyzer in control and irradiated WT pretreated in the presence or absence of a CD47 antisense morpholino (10 μM). *E*, basal OCR was calculated as the area under the curve (*AUC*) for measurements 1–4 and is presented as the mean ± S.D. $n = 3$–4. * denotes $p < 0.01$. *F*, PGC1α mRNA levels were assessed by quantitative RT-PCR and are presented as -fold change relative to untreated WT cells (mean ± S.D., $n = 3$–4, * denotes $p < .01$). *G*, GPX1 mRNA levels were assessed 24 h post-IR by quantitative RT-PCR and are presented as -fold change relative to untreated WT cells (mean ± S.D. $n = 3$; * denotes $p < .01$). *H*, ratios of $NADH/NAD^+$ in control and irradiated WT and CD47(−) cells (mean ± S.E., $n = 2$). *I*, total NAD in control and irradiated WT and CD47(−) cells (mean ± S.E., $n = 2$).

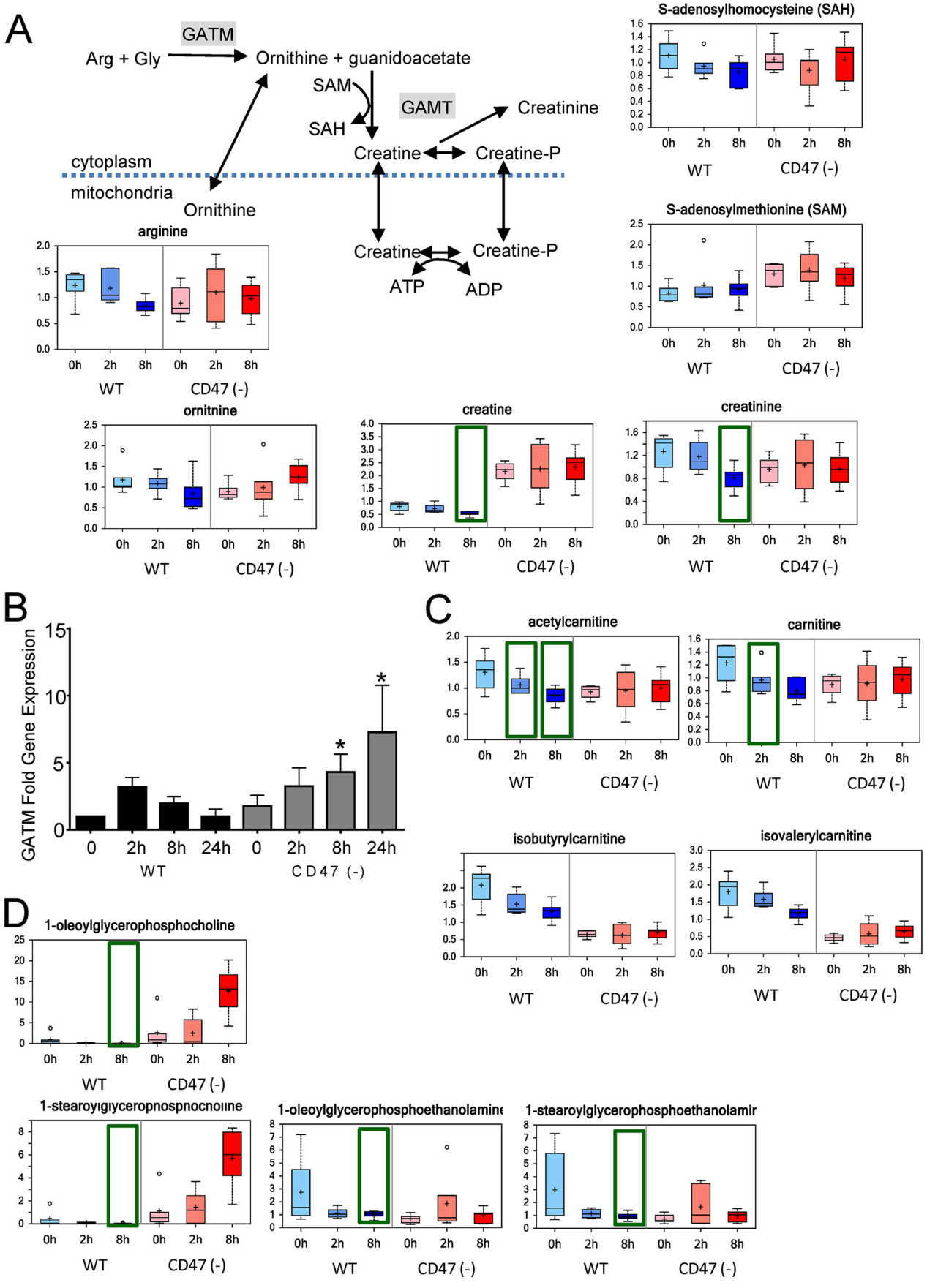
A
GATM
Arg + Gly
Ornithine + guanidoacetate
SAM
SAH
GAMT
Creatinine
Creatine
Creatine-P
cytoplasm
mitochondria
Ornithine
Creatine
Creatine-P
ATP
ADP
S-adenosylhomocysteine (SAH)
S-adenosylmethionine (SAM)
arginine
ornitnine
creatine
creatinine
0h 2h 8h 0h 2h 8h
WT
CD47 (-)
B
GATM Fold Gene Expression
0 2h 8h 24h 0 2h 8h 24h
WT
CD47 (-)
C
acetylcarnitine
carnitine
isobutyrylcarnitine
isovalerylcarnitine
D
1-oleoylglycerophosphocholine
1-stearoylglycerophosphocholine
1-oleoylglycerophosphoethanolamine
1-stearoylglycerophosphoethanolamir

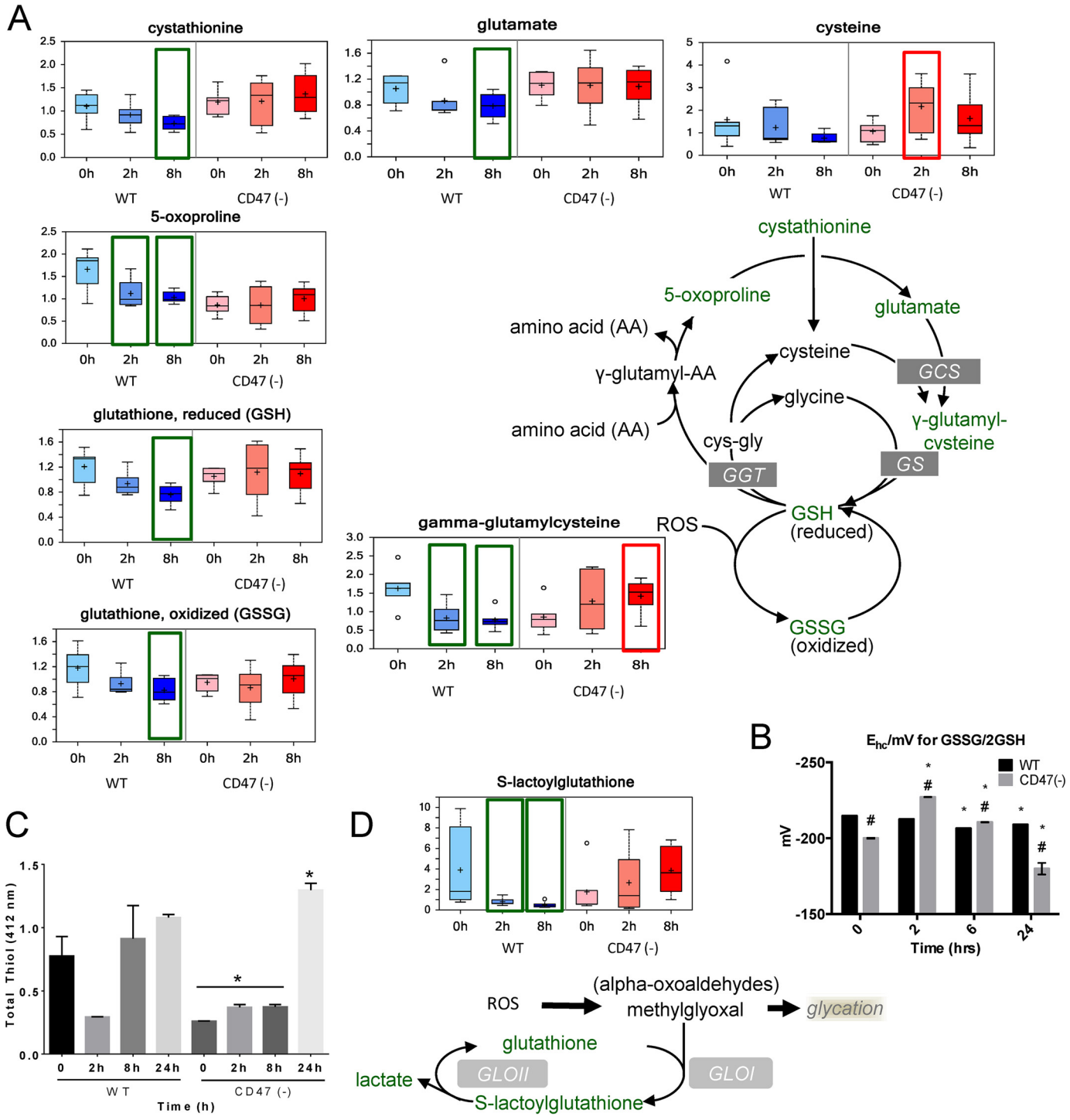

FIGURE 8. **Regulation of reactive oxygen species response pathways by CD47.** *A*, differential regulation of glutathione metabolites in irradiated WT and CD47(−) Jurkat cells. *ROS*, reactive oxygen species. *GS*, glutathione synthetase; *GGT*, γ-glutamyl transpeptidase; *GCS*, γ-glutamyl cysteine synthetase. *B*, cellular chemical potential of the glutathione redox couple in control and irradiated WT and CD47(−) (mean ± S.E., $n = 3$). *C*, free thiol concentrations in the indicated cell lysates were determined by colorimetric assay using Ellman's reagent. *D*, CD47 deficiency preserves the ability of irradiated cells to detoxify α-oxyaldehydes via glyoxalase-1. Baseline (no enzyme) levels were evaluated at 0, 2, 8 and 24 h post-radiation (mean ± S.D., $n = 3$, $p < 0.05$, * relative to time 0, # relative to WT).

FIGURE 7. **Global effects of CD47 signaling on labile methyl group metabolism.** *A*, CD47 deficiency enhances the creatine kinase pathway. Creatine biosynthetic and catabolic metabolites were quantified before and 2 and 8 h after irradiation of WT and CD47(−) Jurkat cells. *SAH*, *S*-adenosylhomocysteine; *SAM*, methionine homocysteine. *B*, GATM mRNA levels were assessed by quantitative RT-PCR and are presented as -fold change relative to untreated WT cells. *C*, carnitine metabolites were quantified before and 2 and 8 h after irradiation of WT and CD47(−) cells. *D*, representative choline and ethanolamine phospholipid metabolites were quantified before and 2 and 8 h after irradiation of WT and CD47(−) cells. *, $p < 0.05$.

A

ANOVA Contrasts		Total biochemicals $p \leq 0.05$	Biochemicals (↑↓)
IR Ctrl	WT	73	42|31
	cd47-/-	52	26|26

B

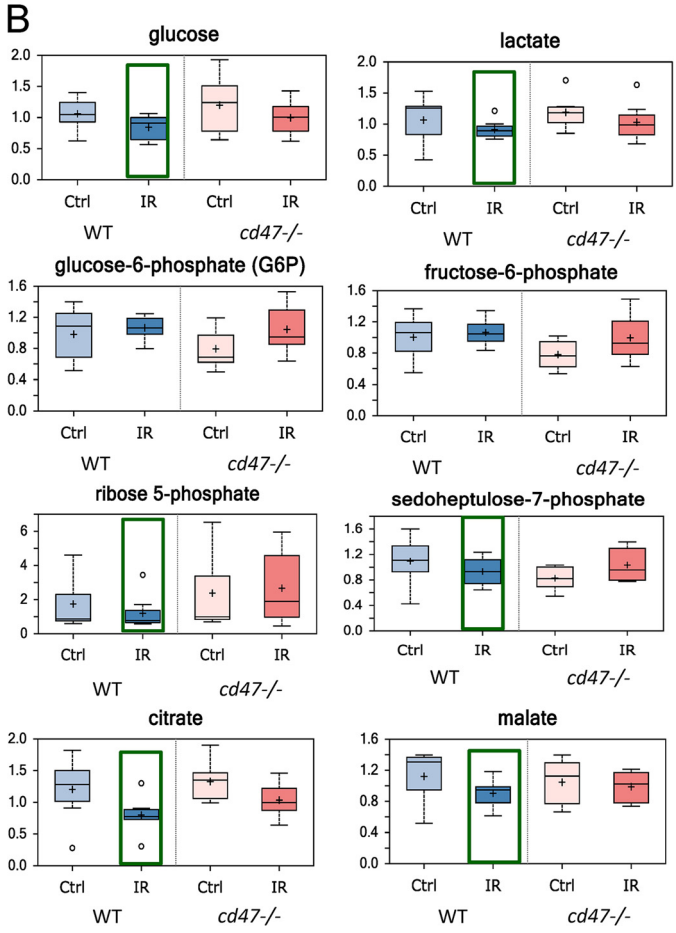

FIGURE 9. **Metabolic responses of WT and *cd47*-null mice to total body irradiation.** *A*, global metabolic responses of lung tissue from WT and *cd47*-null mice exposed to 7.6 Gy total body irradiation. At 24 h post-IR lung tissue was harvested and flash-frozen for metabolomic analysis (n = 7 or 8). Numbers of metabolites significantly altered relative to untreated lung tissue 24 h after irradiation and numbers up- (*red*) or down-regulated (*green*) are presented. *B*, representative metabolite levels at 24 h in lung tissue of WT and *cd47*-null mice exposed to total body irradiation at a dose of 7.6 Gy.

sion of the transcription factor PGC1α (39). PGC1α is further induced by irradiation in CD47(−) but not in WT Jurkat cells and positively regulates several of the genes we found to be selectively induced by irradiation in the CD47(−) cells including Cox5 and Gpx1. Gpx1 is a cytosolic and mitochondrial enzyme that is cytoprotective against oxidative stress, which may contribute to the increased resistance of CD47(−) cells to radiation. Through this and other transcriptional targets, PGC1α inhibits the generation of mitochondrial-driven reactive oxygen species (40), which may contribute to the preservation of a favorable redox environment in irradiated CD47(−) cells. PGC1α positively regulates glucose consumption and ATP levels and decreases lactate excretion in human melanoma cells (53). The latter is consistent with the lower basal intracellular lactate level in WT *versus* CD47(−) cells.

CD47(−) Jurkat cells exhibit elevated expression of c-Myc that is suppressed when CD47 is ligated by thrombospondin-1 (29). c-Myc is a global regulator of cell metabolism (54, 55). Overexpression of c-Myc in pre-B cells increased their glucose uptake, glycolysis, and lactate generation (30). The increased glucose uptake in CD47(−) cells is consistent with this report and their elevated c-Myc expression. The elevated extracellular acidification rate in untreated CD47(−) cells is also consistent with the known stimulation of lactate production by c-Myc. However, elevated intracellular lactate was only observed in the CD47(−) cells relative to WT 8 h after irradiation. Myc also increases the PPP and downstream pyrimidine nucleotide biosynthetic pathways (55). Correspondingly, basal 6-phosphogluconate levels were increased in untreated CD47(−) cells, which would support enhanced nucleotide biosynthesis in irradiated CD47(−) cells.

c-Myc also regulates mitochondrial function. Induction of c-Myc in human B lymphocytes increased oxygen consumption and mitochondrial mass, whereas *Myc*-null cells have decreased mitochondrial mass and numbers (56, 57). Consistent with these observations, CD47(−) T cells have more mitochondria and increased oxygen consumption. Therefore, some of the basal differences in mitochondrial energy metabolism in CD47(−) cells may be direct consequences of their elevated c-Myc expression.

The ability of irradiated CD47(−) cells to maintain total and reduced glutathione levels better than irradiated WT cells is consistent with reports that c-Myc enhances glutamine metabolism via glutaminase, which is limiting for maintenance of cellular glutathione levels and resistance of cells to oxidative stress (58, 59). However, the elevated c-Myc mRNA expression in CD47(−) cells was lost after irradiation, suggesting that additional pathways are involved in the preferential maintenance of reduced glutathione in irradiated CD47(−) cells.

Labile methyl group homeostasis plays multiple roles in cellular responses to stress. 5-Methyl-tetrahydrofolate is required for biosynthesis of thymidine to replace that lost due to DNA damage and is maintained preferentially in irradiated CD47(−) cells. Radiation-induced reactive oxygen species causes extensive oxidative damage to membrane phospholipids, and CD47 regulates the maintenance of one carbon intermediates required to replace damaged phosphatidylcholine. Meeting cytoplasmic energy needs requires the creatine kinase system to shuttle high energy phosphates out of the mitochondria and is also critical for cells to adapt to rapidly changing energy demands (60). CD47(−) cells basally maintain higher creatine levels by controlling levels of the key enzyme in its biosynthesis GATM, and these levels are more resistant to radiation than those in WT cells. Based on the known cytoprotective activity of exogenous creatine for cells exposed to UV irradiation (45) and its utility as a radiation biomarker, we predict that the favorable creatine metabolism in CD47(−) cells contributes to their radioresistance. In addition to its role in mitochondrial lipid oxidation, acetyl carnitine was reported to have a cytoprotective activity that is independent of mitochondrial metabolism and involves preservation of anaerobic glycoly-

sis (61). Selective preservation of acetyl carnitine levels in irradiated CD47(−) cells, therefore, may further enhance their radioresistance.

Viewed globally, CD47 has remarkably pleiotropic effects on cellular responses to the damage caused by IR. It is unlikely that any one of the known signaling pathways controlled by CD47 can account for all of these metabolic responses, but based on evidence that autophagy is necessary for radioprotection of CD47-deficient cells, we predict that autophagy plays a prominent role in global metabolic regulation by CD47. CD47 also plays a number of tissue-specific roles such as regulating blood flow, central blood pressure, platelet hemostasis, and regulating surveillance by phagocytic cells. We propose that modulating global responses to stress constitutes a more universal and evolutionarily ancient function of CD47 signaling. The present data reinforce the therapeutic potential for targeting CD47 to protect or sensitize cells and tissues to IR. Further work will be required to understand why normal and cancerous cells differ in their metabolic responses to CD47 blockade.

Author Contributions—T. W. M., D. R. S.-P., and D. D. R. conceived and coordinated the study and wrote the paper. A. L. S. designed, performed, and analyzed the experiments shown in Figs. 1, 4, and 8. J. M. S. designed, performed, and analyzed the experiments shown in Fig. 6. W. G. D., L. A. R., and D. A. W. provided technical assistance and contributed to writing the paper. All authors reviewed the results and approved the final version of the manuscript.

References

1. Bartek, J., Lukas, J., and Bartkova, J. (2007) DNA damage response as an anti-cancer barrier: damage threshold and the concept of "conditional haploinsufficiency." *Cell Cycle* **6,** 2344–2347
2. Kroemer, G., Mariño, G., and Levine, B. (2010) Autophagy and the integrated stress response. *Mol. Cell* **40,** 280–293
3. Rambold, A. S., and Lippincott-Schwartz, J. (2011) Mechanisms of mitochondria and autophagy crosstalk. *Cell Cycle* **10,** 4032–4038
4. Patterson, A. D., Li, H., Eichler, G. S., Krausz, K. W., Weinstein, J. N., Fornace, A. J., Jr., Gonzalez, F. J., and Idle, J. R. (2008) UPLC-ESI-TOFMS-based metabolomics and gene expression dynamics inspector self-organizing metabolomic maps as tools for understanding the cellular response to ionizing radiation. *Anal. Chem.* **80,** 665–674
5. Wang, C., Yang, J., and Nie, J. (2009) Plasma phospholipid metabolic profiling and biomarkers of rats following radiation exposure based on liquid chromatography-mass spectrometry technique. *Biomed. Chromatogr.* **23,** 1079–1085
6. Varghese, R. S., Cheema, A., Cheema, P., Bourbeau, M., Tuli, L., Zhou, B., Jung, M., Dritschilo, A., and Ressom, H. W. (2010) Analysis of LC-MS data for characterizing the metabolic changes in response to radiation. *J. Proteome Res.* **9,** 2786–2793
7. Lee, R., and Britz-McKibbin, P. (2010) Metabolomic studies of radiation-induced apoptosis of human leukocytes by capillary electrophoresis-mass spectrometry and flow cytometry: adaptive cellular responses to ionizing radiation. *Electrophoresis* **31,** 2328–2337
8. Khan, A. R., Rana, P., Devi, M. M., Chaturvedi, S., Javed, S., Tripathi, R. P., and Khushu, S. (2011) Nuclear magnetic resonance spectroscopy-based metabonomic investigation of biochemical effects in serum of γ-irradiated mice. *Int. J. Radiat. Biol.* **87,** 91–97
9. Tyburski, J. B., Patterson, A. D., Krausz, K. W., Slavík, J., Fornace, A. J., Jr., Gonzalez, F. J., and Idle, J. R. (2009) Radiation metabolomics. 2. dose- and time-dependent urinary excretion of deaminated purines and pyrimidines after sublethal γ-radiation exposure in mice. *Radiat. Res.* **172,** 42–57
10. Johnson, C. H., Patterson, A. D., Krausz, K. W., Lanz, C., Kang, D. W., Luecke, H., Gonzalez, F. J., and Idle, J. R. (2011) Radiation metabolomics. 4. UPLC-ESI-QTOFMS-Based metabolomics for urinary biomarker discovery in γ-irradiated rats. *Radiat. Res.* **175,** 473–484
11. Johnson, C. H., Patterson, A. D., Krausz, K. W., Kalinich, J. F., Tyburski, J. B., Kang, D. W., Luecke, H., Gonzalez, F. J., Blakely, W. F., and Idle, J. R. (2012) Radiation metabolomics. 5. Identification of urinary biomarkers of ionizing radiation exposure in nonhuman primates by mass spectrometry-based metabolomics. *Radiat. Res.* **178,** 328–340
12. Ghosh, S. P., Singh, R., Chakraborty, K., Kulkarni, S., Uppal, A., Luo, Y., Kaur, P., Pathak, R., Kumar, K. S., Hauer-Jensen, M., and Cheema, A. K. (2013) Metabolomic changes in gastrointestinal tissues after whole body radiation in a murine model. *Mol. Biosyst.* **9,** 723–731
13. Lee, E. J., Gerhold, M., Palmer, M. W., and Christen, R. D. (2003) p53 protein regulates the effects of amifostine on apoptosis, cell cycle progression, and cytoprotection. *Br. J. Cancer* **88,** 754–759
14. Bourhis, J., Blanchard, P., Maillard, E., Brizel, D. M., Movsas, B., Buentzel, J., Langendijk, J. A., Komaki, R., Swan Leong, S., Levendag, P., and Pignon, J. P. (2011) Effect of amifostine on survival among patients treated with radiotherapy: a meta-analysis of individual patient data. *J. Clin. Oncol.* **29,** 2590–2597
15. von Bueren, A. O., Oehler, C., Shalaby, T., von Hoff, K., Pruschy, M., Seifert, B., Gerber, N. U., Warmuth-Metz, M., Stearns, D., Eberhart, C. G., Kortmann, R. D., Rutkowski, S., and Grotzer, M. A. (2011) c-MYC expression sensitizes medulloblastoma cells to radio- and chemotherapy and has no impact on response in medulloblastoma patients. *BMC Cancer* **11,** 74
16. Hara, T., Omura-Minamisawa, M., Kang, Y., Cheng, C., and Inoue, T. (2008) Flavopiridol potentiates the cytotoxic effects of radiation in radioresistant tumor cells in which p53 is mutated or Bcl-2 is overexpressed. *Int. J. Radiat. Oncol. Biol. Phys.* **71,** 1485–1495
17. Truman, J. P., Rotenberg, S. A., Kang, J. H., Lerman, G., Fuks, Z., Kolesnick, R., Marquez, V. E., and Haimovitz-Friedman, A. (2009) PKCα activation downregulates ATM and radio-sensitizes androgen-sensitive human prostate cancer cells *in vitro* and *in vivo*. *Cancer Biol. Ther.* **8,** 54–63
18. Roberts, D. D., Miller, T. W., Rogers, N. M., Yao, M., and Isenberg, J. S. (2012) The matricellular protein thrombospondin-1 globally regulates cardiovascular function and responses to stress. *Matrix Biol.* **31,** 162–169
19. Isenberg, J. S., Maxhimer, J. B., Hyodo, F., Pendrak, M. L., Ridnour, L. A., DeGraff, W. G., Tsokos, M., Wink, D. A., and Roberts, D. D. (2008) Thrombospondin-1 and CD47 limit cell and tissue survival of radiation injury. *Am. J. Pathol.* **173,** 1100–1112
20. Maxhimer, J. B., Soto-Pantoja, D. R., Ridnour, L. A., Shih, H. B., Degraff, W. G., Tsokos, M., Wink, D. A., Isenberg, J. S., and Roberts, D. D. (2009) Radioprotection in normal tissue and delayed tumor growth by blockade of CD47 signaling. *Sci. Transl. Med.* **1,** 3ra7
21. Soto-Pantoja, D. R., Ridnour, L. A., Wink, D. A., and Roberts, D. D. (2013) Blockade of CD47 increases survival of mice exposed to lethal total body irradiation. *Sci. Rep.* **3,** 1038
22. Soto-Pantoja, D. R., Miller, T. W., Pendrak, M. L., DeGraff, W. G., Sullivan, C., Ridnour, L. A., Abu-Asab, M., Wink, D. A., Tsokos, M., and Roberts, D. D. (2012) CD47 deficiency confers cell and tissue radioprotection by activation of autophagy. *Autophagy* **8,** 1628–1642
23. Soto-Pantoja, D. R., Terabe, M., Ghosh, A., Ridnour, L. A., DeGraff, W. G., Wink, D. A., Berzofsky, J. A., and Roberts, D. D. (2014) CD47 in the tumor microenvironment limits cooperation between antitumor T-cell immunity and radiotherapy. *Cancer Res.* **74,** 6771–6783
24. Reinhold, M. I., Green, J. M., Lindberg, F. P., Ticchioni, M., and Brown, E. J. (1999) Cell spreading distinguishes the mechanism of augmentation of T cell activation by integrin-associated protein/CD47 and CD28. *Int. Immunol.* **11,** 707–718
25. Lindberg, F. P., Bullard, D. C., Caver, T. E., Gresham, H. D., Beaudet, A. L., and Brown, E. J. (1996) Decreased resistance to bacterial infection and granulocyte defects in IAP-deficient mice. *Science* **274,** 795–798
26. Reitman, Z. J., Jin, G., Karoly, E. D., Spasojevic, I., Yang, J., Kinzler, K. W., He, Y., Bigner, D. D., Vogelstein, B., and Yan, H. (2011) Profiling the effects of isocitrate dehydrogenase 1 and 2 mutations on the cellular metabolome. *Proc. Natl. Acad. Sci. U.S.A.* **108,** 3270–3275
27. Evans, A. M., DeHaven, C. D., Barrett, T., Mitchell, M., and Milgram, E. (2009) Integrated, nontargeted ultrahigh performance liquid chromatography/electrospray ionization tandem mass spectrometry platform for the

identification and relative quantification of the small-molecule complement of biological systems. *Anal. Chem.* **81,** 6656–6667
28. Fujibayashi, Y., Waki, A., Sakahara, H., Konishi, J., Yonekura, Y., Ishii, Y., and Yokoyama, A. (1997) Transient increase in glycolytic metabolism in cultured tumor cells immediately after exposure to ionizing radiation: from gene expression to deoxyglucose uptake. *Radiat. Res.* **147,** 729–734
29. Kaur, S., Soto-Pantoja, D. R., Stein, E. V., Liu, C., Elkahloun, A. G., Pendrak, M. L., Nicolae, A., Singh, S. P., Nie, Z., Levens, D., Isenberg, J. S., and Roberts, D. D. (2013) Thrombospondin-1 signaling through CD47 inhibits self-renewal by regulating c-Myc and other stem cell transcription factors. *Sci. Rep.* **3,** 1673
30. Fan, Y., Dickman, K. G., and Zong, W. X. (2010) Akt and c-Myc differentially activate cellular metabolic programs and prime cells to bioenergetic inhibition. *J. Biol. Chem.* **285,** 7324–7333
31. Miccheli, A., Tomassini, A., Puccetti, C., Valerio, M., Peluso, G., Tuccillo, F., Calvani, M., Manetti, C., and Conti, F. (2006) Metabolic profiling by 13C-NMR spectroscopy: [1,2–13C2]glucose reveals a heterogeneous metabolism in human leukemia T cells. *Biochimie* **88,** 437–448
32. Prignitz, R., Hoffmeister, N., and Hoffmeister, G. (1975) [Studies on the effect of radiation on electrolyte changes and metabolism of the myocardium. V. Changes in enzyme activities and glycolysis metabloites due to radiation]. *Strahlentherapie* **149,** 621–627
33. Endoh, K., Murakami, M., Araki, R., Maruyama, C., and Umegaki, K. (2006) Low folate status increases chromosomal damage by x-ray irradiation. *Int. J. Radiat. Biol.* **82,** 223–230
34. Gupta, G. S., and Bawa, S. R. (1977) Radiation effects on testes. X. Studies on inorganic pyrophosphatase and pyrophosphate following γ irradiation of rats. *Radiat. Res.* **71,** 83–96
35. Zempleni, J., Teixeira, D. C., Kuroishi, T., Cordonier, E. L., and Baier, S. (2012) Biotin requirements for DNA damage prevention. *Mutat. Res.* **733,** 58–60
36. Hoosein, M. A., and Lewin, A. S. (1984) Derepression of citrate synthase in *Saccharomyces cerevisiae* may occur at the level of transcription. *Mol. Cell. Biol.* **4,** 247–253
37. Yao, X., Zeng, M., Wang, H., Fei, S., Rao, S., and Ji, Y. (2012) Metabolite detection of pancreatic carcinoma by *in vivo* proton MR spectroscopy at 3T: initial results. *Radiol. Med.* **117,** 780–788
38. Collard, F., Vertommen, D., Constantinescu, S., Buts, L., and Van Schaftingen, E. (2011) Molecular identification of β-citrylglutamate hydrolase as glutamate carboxypeptidase 3. *J. Biol. Chem.* **286,** 38220–38230
39. Frazier, E. P., Isenberg, J. S., Shiva, S., Zhao, L., Schlesinger, P., Dimitry, J., Abu-Asab, M. S., Tsokos, M., Roberts, D. D., and Frazier, W. A. (2011) Age-dependent regulation of skeletal muscle mitochondria by the thrombospondin-1 receptor CD47. *Matrix Biol.* **30,** 154–161
40. St-Pierre, J., Drori, S., Uldry, M., Silvaggi, J. M., Rhee, J., Jäger, S., Handschin, C., Zheng, K., Lin, J., Yang, W., Simon, D. K., Bachoo, R., and Spiegelman, B. M. (2006) Suppression of reactive oxygen species and neurodegeneration by the PGC-1 transcriptional coactivators. *Cell* **127,** 397–408
41. Tsunemi, T., Ashe, T. D., Morrison, B. E., Soriano, K. R., Au, J., Roque, R. A., Lazarowski, E. R., Damian, V. A., Masliah, E., and La Spada, A. R. (2012) PGC-1α rescues Huntington's disease proteotoxicity by preventing oxidative stress and promoting TFEB function. *Sci. Transl. Med.* **4,** 142ra197
42. Wyss, M., and Kaddurah-Daouk, R. (2000) Creatine and creatinine metabolism. *Physiol. Rev.* **80,** 1107–1213
43. Gerber, G. B., Gerbert, G., Koszalka, T. R., and Hempelmann, L. H. (1964) Creatine Metabolism after x-irradiation of Rats. Ii. Direct and indirect effect of radiation. *Radiat. Res.* **23,** 648–652
44. Basu, S. K., Srinivasan, M. N., Chuttani, K., Bhatnagar, A., and Ghose, A. (1985) Urinary excretion of creatine and creatinine in γ irradiated rats. *J. Radiat. Res.* **26,** 189–195
45. Lenz, H., Schmidt, M., Welge, V., Schlattner, U., Wallimann, T., Elsässer, H. P., Wittern, K. P., Wenck, H., Stäb, F., and Blatt, T. (2005) The creatine kinase system in human skin: protective effects of creatine against oxidative and UV damage *in vitro* and *in vivo*. *J. Invest. Dermatol.* **124,** 443–452
46. Mudd, S. H., Brosnan, J. T., Brosnan, M. E., Jacobs, R. L., Stabler, S. P., Allen, R. H., Vance, D. E., and Wagner, C. (2007) Methyl balance and transmethylation fluxes in humans. *Am. J. Clin. Nutr.* **85,** 19–25
47. Schafer, F. Q., and Buettner, G. R. (2001) Redox environment of the cell as viewed through the redox state of the glutathione disulfide/glutathione couple. *Free Radic Biol. Med.* **30,** 1191–1212
48. Lin, X., Zhang, F., Bradbury, C. M., Kaushal, A., Li, L., Spitz, D. R., Aft, R. L., and Gius, D. (2003) 2-Deoxy-D-glucose-induced cytotoxicity and radiosensitization in tumor cells is mediated via disruptions in thiol metabolism. *Cancer Res.* **63,** 3413–3417
49. Sharma, R., and Kale, R. K. (1993) Effect of radiation on glyoxalase I and glyoxalase II activities in spleen and liver of mice. *Int. J. Radiat. Biol.* **63,** 233–238
50. Soto-Pantoja, D. R., Kaur, S., and Roberts, D. D. (2015) CD47 signaling pathways controlling cellular differentiation and responses to stress. *Crit. Rev. Biochem. Mol. Biol.* **50,** 212–230
51. Rabinowitz, J. D., and White, E. (2010) Autophagy and metabolism. *Science* **330,** 1344–1348
52. Müller, T. D., Lee, S. J., Jastroch, M., Kabra, D., Stemmer, K., Aichler, M., Abplanalp, B., Ananthakrishnan, G., Bhardwaj, N., Collins, S., Divanovic, S., Endele, M., Finan, B., Gao, Y., Habegger, K. M., Hembree, J., Heppner, K. M., Hofmann, S., Holland, J., Küchler, D., Kutschke, M., Krishna, R., Lehti, M., Oelkrug, R., Ottaway, N., Perez-Tilve, D., Raver, C., Walch, A. K., Schriever, S. C., Speakman, J., Tseng, Y. H., Diaz-Meco, M., Pfluger, P. T., Moscat, J., and Tschöp, M. H. (2013) p62 links β-adrenergic input to mitochondrial function and thermogenesis. *J. Clin. Invest.* **123,** 469–478
53. Vazquez, F., Lim, J. H., Chim, H., Bhalla, K., Girnun, G., Pierce, K., Clish, C. B., Granter, S. R., Widlund, H. R., Spiegelman, B. M., and Puigserver, P. (2013) PGC1α expression defines a subset of human melanoma tumors with increased mitochondrial capacity and resistance to oxidative stress. *Cancer Cell* **23,** 287–301
54. Gordan, J. D., Thompson, C. B., and Simon, M. C. (2007) HIF and c-Myc: sibling rivals for control of cancer cell metabolism and proliferation. *Cancer Cell* **12,** 108–113
55. Morrish, F., Isern, N., Sadilek, M., Jeffrey, M., and Hockenbery, D. M. (2009) c-Myc activates multiple metabolic networks to generate substrates for cell-cycle entry. *Oncogene* **28,** 2485–2491
56. Li, F., Wang, Y., Zeller, K. I., Potter, J. J., Wonsey, D. R., O'Donnell, K. A., Kim, J. W., Yustein, J. T., Lee, L. A., and Dang, C. V. (2005) Myc stimulates nuclearly encoded mitochondrial genes and mitochondrial biogenesis. *Mol. Cell. Biol.* **25,** 6225–6234
57. Kim, J., Lee, J. H., and Iyer, V. R. (2008) Global identification of Myc target genes reveals its direct role in mitochondrial biogenesis and its E-box usage *in vivo*. *PLoS ONE* **3,** e1798
58. Gao, P., Tchernyshyov, I., Chang, T. C., Lee, Y. S., Kita, K., Ochi, T., Zeller, K. I., De Marzo, A. M., Van Eyk, J. E., Mendell, J. T., and Dang, C. V. (2009) c-Myc suppression of miR-23a/b enhances mitochondrial glutaminase expression and glutamine metabolism. *Nature* **458,** 762–765
59. Lora, J., Alonso, F. J., Segura, J. A., Lobo, C., Márquez, J., and Matés, J. M. (2004) Antisense glutaminase inhibition decreases glutathione antioxidant capacity and increases apoptosis in Ehrlich ascitic tumour cells. *Eur. J. Biochem.* **271,** 4298–4306
60. Wallimann, T., Tokarska-Schlattner, M., and Schlattner, U. (2011) The creatine kinase system and pleiotropic effects of creatine. *Amino Acids* **40,** 1271–1296
61. Mazzio, E., Yoon, K. J., and Soliman, K. F. (2003) Acetyl-L-carnitine cytoprotection against 1-methyl-4-phenylpyridinium toxicity in neuroblastoma cells. *Biochem. Pharmacol.* **66,** 297–306